11-8-2007

Mechanical Properties of Silicon Carbide (SiC) Thin Films

Jayadeep Deva Reddy
University of South Florida

Mechanical Properties of Silicon Carbide (SiC) Thin Films

by

Jayadeep Deva Reddy

A thesis submitted in partial fulfillment
of the requirements for the degree of
Master of Science in Mechanical Engineering
Department of Mechanical Engineering
College of Engineering
University of South Florida

Major Professor: Alex A. Volinsky, Ph.D.
Ashok Kumar, Ph.D.
Nathan B. Crane, Ph.D.

Date of Approval:
November 8, 2007

Keywords: nanoindentation, hardness, elastic modulus, fracture toughness, hertzian contact theory

TABLE OF CONTENTS

LIST OF TABLES

LIST OF FIGURES

MECHANICAL PROPERTIES OF SILICON CARBIDE (SIC) THIN FILMS

Jayadeep Deva Reddy

ABSTRACT

There is a technological need for hard thin films with high elastic modulus. Silicon Carbide (SiC) fulfills such requirements with a variety of applications in high temperature and MEMS devices. A detailed study of SiC thin films mechanical properties was performed by means of nanoindentation. The report is on the comparative studies of the mechanical properties of epitaxially grown cubic (3C) single crystalline and polycrystalline SiC thin films on Si substrates. The thickness of both the Single and polycrystalline SiC samples were around 1-2 μm. Under indentation loads below 500 μN both films exhibit Elastic contact without plastic deformation. Based on the nanoindentation results polycrystalline SiC thin films have an elastic modulus and hardness of 422 $\pm$ 16 GPa and 32.69 $\pm$ 3.218 GPa respectively, while single crystalline SiC films elastic modulus and hardness of 410 $\pm$ 3.18 Gpa and 30 $\pm$ 2.8 Gpa respectively. Fracture toughness experiments were also carried out using the nanoindentation technique and values were measured to be 1.48 ± 0.6 GPa for polycrystalline SiC and 1.58 ± 0.5 GPa for single crystal SiC, respectively. These results show that both polycrystalline SiC thin films and single crystal SiC more or less have similar properties. Hence both single crystal and polycrystalline SiC thin films have the capability of

becoming strong contenders for MEMS applications, as well as hard and protective coatings for cutting tools and coatings for MEMS devices.

CHAPTER 1

1.1 Introduction

This chapter discusses in detail silicon carbide (SiC), hard coatings, thin films in MEMS devices, thin film deposition by Chemical vapor deposition (CVD) and advantages of CVD.

1.2 An Overview of Silicon Carbide

Silicon Carbide (SiC) has been used increasingly in electronic devices and Micro-Electro-Mechanical Systems (MEMS) due to its capability of operating at high power levels and high temperatures. Another area that has benefited from the development of thin film technology is in the development of metallurgical and protective coatings [1, 2]. One of the challenges in micro level devices is providing corrosion resistance for such environments as biological systems or caustic gases. Silicon Carbide has been recognized as an ideal material for applications that require superior hardness, high thermal conductivity, low thermal expansion, chemical and oxidation resistance. Klumpp et. al. were the first to recognize the potential of silicon carbide for use in MEMS devices in 1994 [3]. Since then, it has been used as protective coatings in harsh environment [3, 4]. Silicon carbide is a wide band gap semiconductor of choice for high-power, high

frequency and high temperature devices, due to its high breakdown field; high electron saturated drift velocity and good thermal conductivity.

SiC is a wide band gap semiconductor. It exists in many different polytypes. All polytypes have a hexagonal frame with a carbon atom situated above the center of a triangle of Si atoms and underneath a Si atom belonging to the next layer. The distance, marked as 'a' in Figure 1.1, between neighboring silicon or carbon atoms is approximately 3.08 Å for all polytypes, 'C-Si' is approximately 1.89 Å**.**

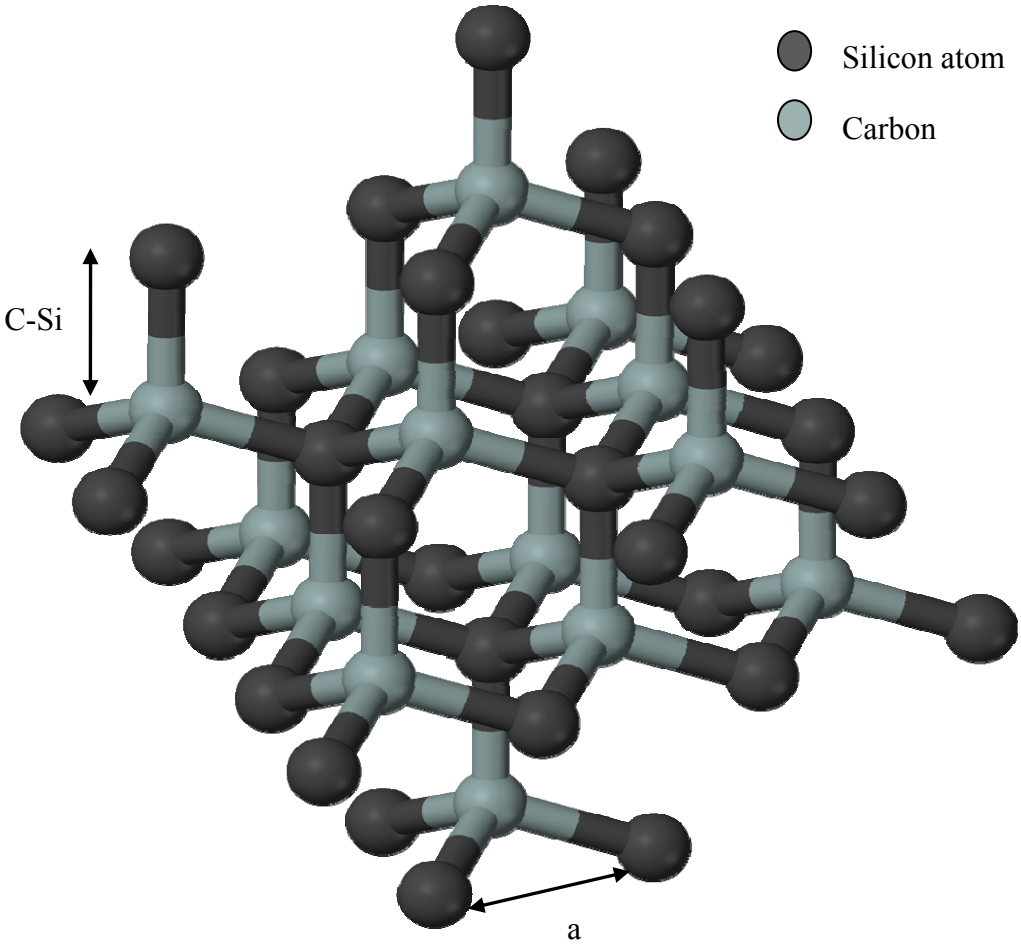

Figure 1.1. The Tetragonal Bonding of a Carbon Atom With the Four Nearest Silicon Neighbors

The carbon atom is the center atom of a tetrahedral structure surrounded by four Si atoms; and the distance between the C atom and each Si atom (marked as C-Si in Figure 1.1) is the same.

The stacking sequence is shown in Figure 1.2 for the four most common polytypes, 3C, 2H, 4H and 6H. There are three different layers referred to as A, B, and C in Figure 1.2. If the first layer is A, the next layer according to a closed packed structure will be layer B or C. The different polytypes can be constructed by any combination of these three layers. The 3C-SiC polytype is the only cubic polytype and it has a stacking sequence ABCABC… or ACBACB…

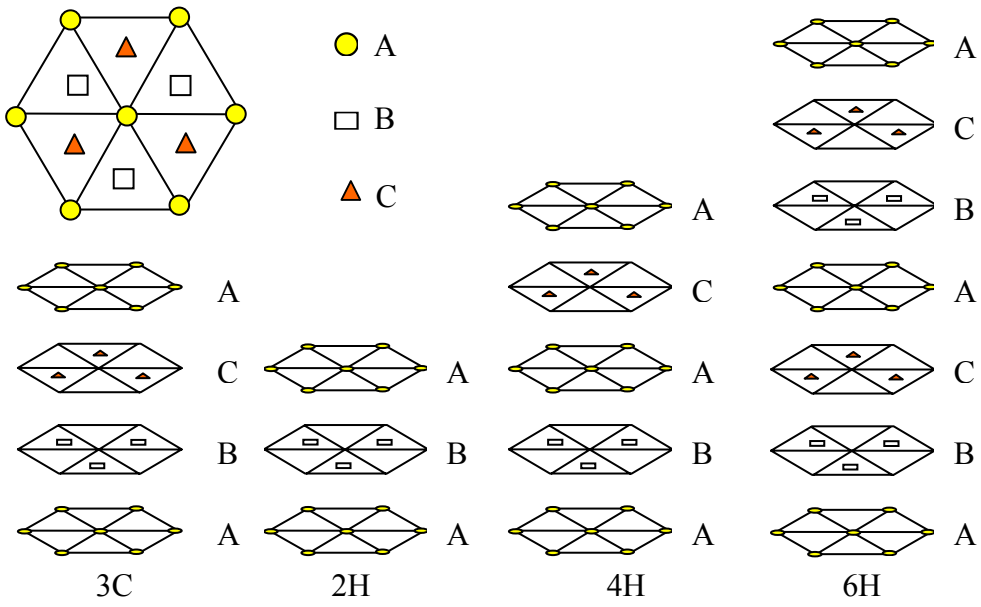

Figure 1.2. The Stacking Sequence of Double Layers in Most Common SiC Polytypes

The performance of SiC due to its high-temperature, and high-power capabilities makes it suitable for aircraft, automotive, communications, power, and spacecraft industries. These specific industries are starting to take advantage of the benefits of SiC in electronics. SiC films are used as high temperature semiconductors [5].

Thin films have several applications due to their improved mechanical properties, protection against chemical environments, radiation and mechanical wear. On the other hand thin films have been used due to their electrical and optical properties. SiC is suitable for both of these applications.

1.3 Hard Coatings

Hardness is an important property for thin films used in electronic, optical, and mechanical applications. Harder coatings also have higher wear resistance, also harder surfaces tend to have lower friction and lubrication has better results with harder surfaces [1]. Silicon carbide is covalently bonded, which is the reason for its high hardness.

Hard coatings have been used successfully for two decades to protective materials, and to increase the lifetime and efficiency of cutting tools. Hard coated surfaces have been used to reduce the problems of chemical diffusion, wear, friction, oxidation and corrosion and effectively increase the life of the lithographie-galvanoformung-abformung (LIGA) microdevices [6-8] and other sensitive devices. Recently the performance and reliability of MEMS components were enhanced dramatically through the incorporation of protective thin-film coatings [9]. SiC hard coatings have helped to increase the efficiency of MEMS devices by protecting them from harsh environmental conditions.

1.4 Thin Films for MEMS Devices

Most MEMS devices are restricted due to low operation temperatures, for example silicon devices are restricted to a maximum temperature of 250 ^{0}C and can be easily affected chemically. SiC is known for high thermal conductivity and electrical stability at temperatures higher than 300 ^{0}C [10]. This has been a vital breakthrough for reliability of MEMS devices in harsh environments.

1.5 Thin Film Deposition

There are various techniques for depositing thin films which can have a major affect on the mechanical properties of the film. The most common methods of depositing thin films are Physical Vapor Deposition (PVD) and Chemical Vapor Deposition (CVD). The main PVD processes are evaporation and sputtering. The CVD process involves making a volatile compound react with a material to be deposited with other gases; in this process a non-volatile solid gets deposited on a suitably placed substrate. SiC thin films can be deposited by CVD. A variety of carbide, nitride, boride films and coatings can also be deposited by this method [1].

Physical vapor deposition (PVD) is a general term used to describe methods to deposit thin films by the condensation of a vapor onto the surfaces such as semiconductor wafers. This process involves evaporation at high temperature in a vacuum, or plasma sputter bombardment. In this chapter we focus mainly on the CVD process.

1.5.1 Chemical Vapor Deposition (CVD)

CVD is a relatively old technique. The formation of soot due to incomplete oxidation of firewood since prehistoric times is probably the oldest example of CVD deposition. The industrial use of CVD could be traced back to a patent literature by de Lodyguine in 1893, who had deposited W onto carbon lamp filaments through the reduction of WCl_6 by H_2. Around this period, the CVD process was developed as an economically viable industrial process in the field of extraction and pyrometallurgy for the production of high purity refractory metals such as Ti, Ni, Zr and Ta.

One of the important commercial reactions in CVD is:

$$SiCl_{4(g)} + CH_{4(g)} \rightarrow SiC_{(s)} + 4HCl_{(g)} \quad (1400\ ^{\circ}C)$$

for depositing hard wear resistant SiC surface coating.

1.5.2 CVD Mechanism

CVD can be performed in a 'closed' or 'open' system. In the 'closed' system, both reactants and products are recycled. This process is normally used where reversible chemical reactions can occur with a temperature difference. There is no universal CVD or standard CVD. Each piece of CVD equipment is individually tailored for specific coating materials, substrate geometry, etc., whether it is used for R&D or commercial production. In general, the CVD equipment consists of three main components:

- Chemical vapor precursor supply system,
- CVD reactor,

- Affluent gas handling system.

The CVD equipment is designed and operated using optimum processing conditions to provide coating with uniform thickness, surface morphology, structure and composition. Suitable designs have taken into consideration the temperature control, reactant depletion, fluid dynamics and heat transfer in the system [11].

In general, the CVD process involves the following key steps:

- Generation of active gaseous reactant species;
- Transport of the gaseous species into the reaction chamber;
- Gaseous reactants undergo gas phase reactions forming intermediate species:
  - at a high temperature above the decomposition temperatures of intermediate species inside the reactor. Homogeneous gas phase reaction can occur where the intermediate species undergo subsequent decomposition and/or chemical reaction, forming powders and volatile by-products in the gas phase. The powder will be collected on the substrate surface and may act as crystallization centers, and the by-products are transported away from the deposition chamber.
  - at temperatures below the dissociation of the intermediate phase, diffusion/convection of the intermediate species across the boundary layer (a thin layer close to the substrate surface) occurs. These intermediate species subsequently undergo the following steps:
    - Absorption of gaseous reactants onto the heated substrate, followed by heterogeneous reaction at the gas–solid interface (i.e. heated substrate) which produces the deposit and by-product species. The

deposits will diffuse along the heated substrate surface forming crystallization centers followed by film growth.

- Gaseous by-products are removed from the boundary layer through diffusion or convection. The unreacted gaseous precursors and by-products will be transported away from the deposition chamber [11].

1.5.3 Advantages of CVD

CVD has the following distinctive advantages over other methods:

- It has the capability of producing highly dense and pure materials.
- CVD method has high reproducibility and deposits films uniformly at a reasonable deposition rates. It can be used to uniformly coat complex shaped components and deposit films with good conformal coverage. Such distinctive feature outweighs the PVD process.
- It has the ability to control crystal structure, surface morphology and orientation of the CVD products by controlling the CVD process parameters like temperature of the system, flow of precursor gas, and flow of carrier gas.
- Rate of deposition can be easily controlled. CVD at lower deposition rates yields epitaxial thin films for MEMS applications. For thick protective coatings, a high deposition rate is preferred and the deposition rates can be tens of μm per hour. Many techniques cannot achieve higher deposition rates, except plasma spraying.
- CVD is more economical in the field of thin film technology compared to other techniques.

- CVD allows the deposition of a large spectrum of materials including, metals, carbides, nitrides, oxides, sulfides, III–V and II–VI materials by using a wide range of chemical precursors such as halides, hydrides, and organometallics.
- Relatively low deposition temperatures and the desired phases can be deposited in-situ at low energies through vapor phase reactions, and nucleation and growth on the substrate surface. This enables the deposition of refractory materials at a small fraction of their melting temperatures. Silicon carbide can be deposited at a lower temperature of 1000 ^{0}C using chemical reactions rather than doing it at higher temperatures.
- Relatively low deposition temperatures and energies. Using CVD the desired phases can be deposited in-situ at low energies through vapor phase reactions, and nucleation and growth on the substrate surface. This enables the deposition of refractory materials at a small fraction of their melting temperatures. Silicon carbide for example can be deposited at a temperature of 1000 ^{0}C using chemical reactions; this is less than temperatures used on other processes.

Table 1, shows important properties of SiC and compares them to other MEMS materials. Among the materials of interest SiC has a better thermal conductivity, Hardness, Young's Modulus and physical stability compared to Silicon or Gallium Arsenide. These properties give an advantage to SiC thin films. It can be noted from the table that SiC has a reasonably high electron mobility and large bandgap. SiC devices have been effectively operating at higher temperatures up to 600 °C, while the most commonly used and available semiconductor Si could operate only at temperatures of around 200 °C [1, 2]. These properties make SiC more appealing in the field of MEMS, hard coatings, medical

applications, biotechnology, chemical sensors and other electronic applications. The advantages of SiC over the other MEMS material has led to more research in the recent years.

Table 1. Properties of MEMS Materials

Properties/ Material	3C-SiC	Si	GaAs	Diamond
Bandgap Eg (eV)	2.4	1.1	1.4	5.5
Thermal Conductivity (W/cm°C)	5	1.5	0.5	20
Thermal Expansion (10^{-5} / °C)	4.2	2.6	6.88	1
Hardness (GPa)	35-45	12	7	70-80
Electron Mobility (cm^2/ Vs)	1000	1400	8500	2200
Young's Modulus (GPa)	448	190	75	1041
Physical Stability	Excellent	Good	Fair	Excellent
Breakdown Voltage (10^5 V/ cm)	4	0.3	0.4	10

1.6 Research Objective

The main objective and goal of the present research is to determine the mechanical properties of the single crystal and polycrystalline SiC thin films.

CHAPTER 2

2.1 Mechanical Characterization of Thin Films

The main objective of this chapter is to review various methods used for thin film mechanical characterization. There is a large variation in the mechanical properties of thin films due to various conditions in the deposition process among other factors. To increase the lifetime and reliability while maintaining cost effectiveness, characterization of mechanical properties is necessary.

Mechanical properties measurements play an important role in thin film industries because the properties of thin films can differ substantially from the bulk mechanical properties [13, 14]. In recent years there has been considerable interest in the mechanical properties of materials at the micro and nano scales. This is motivated partly by interest in inherently small structures such as thin film systems, Micro Electro Mechanical Systems (MEMS), and small-scale composites, and partly by newly available methods of measuring local mechanical properties in small volumes [15]. The test techniques that were used to determine the mechanical properties of the bulk materials cannot be directly applied to measure the mechanical properties of thin films. Therefore, several new methods have been developed to study the mechanical properties of thin films, which include the bulge test, micro tensile testing, beam deflection techniques, nanoindentation or depth sensing technique and resonance testing to name a few.

2.1.1 Bulge Test

The Bulge test is one of the most versatile tests. It can be used to characterize the residual stress, elastic modulus, and other important parameters such as yield strength and fracture toughness. Bulge testing is one of the most promising testing methods to determine the Young's modulus, residual stress and Poison's ratio. In Bulge testing the substrate is locally removed by etching, and a thin film diaphragm is left behind. The basic principle of the bulge test is to pressurize the diaphragm up to the desired maximum pressure, and observe interference patterns on the bulging film [16].

Figure 2.1, shows a schematic for the experimental setup of the bulge test. Pressure is applied to obtain the load-deflection response. The film whose properties are to be measured is placed on top of the chuck and adhered strongly using hard wax or epoxy. A pressure manifold is attached to the chuck through the minute hole provided. As pressure is applied the film deflects and fringes are formed as shown in Figure 2.2. These fringes are observed through the lens of the microscope/interferometer placed on top of the bulging film. Now, the pressure is gradually decreased to atmospheric level, during the decrease in the pressure the number of fringes that were formed also decreases. With each decreasing fringe, the pressure is recorded, and load versus deflection graphs are plotted.

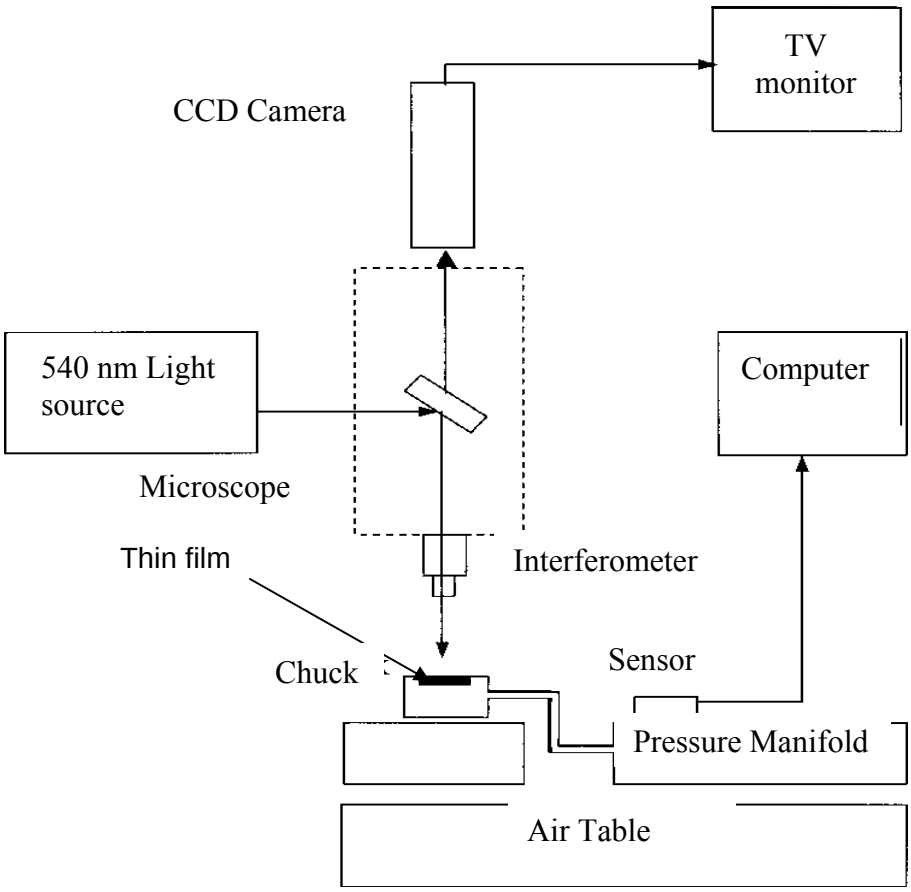

Figure 2.1. Schematic Representation of Bulge Testing Experimental Setup

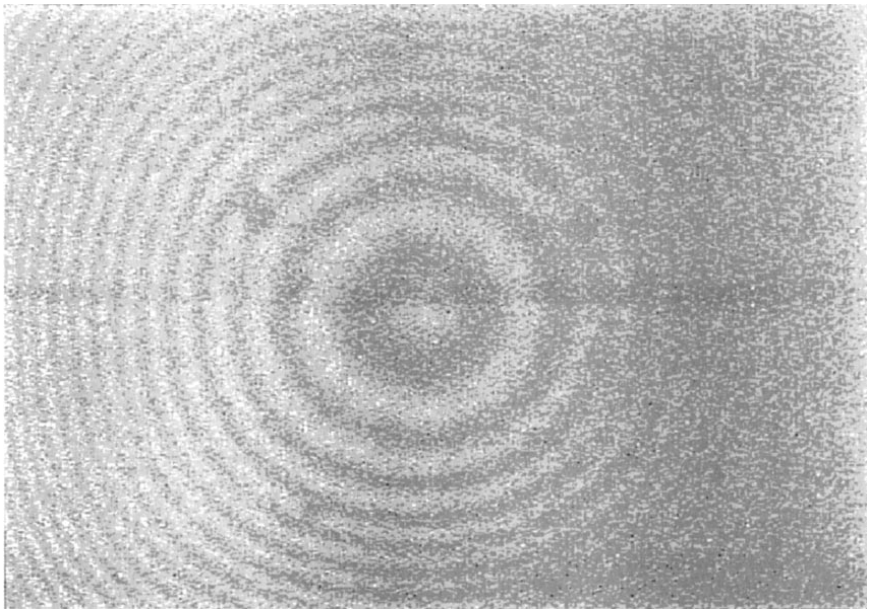

Figure 2.2. Circular Interference Patterns Used to Measure Deflection of Bulging Film [16]

Using the bulge test, the deflection of the thin film is measured as a function of applied pressure. The residual stress and Young's modulus *E* values are then extracted from the linear and cubic coefficients of equation (1). Using a least-square fit, equation (1) can be used to extract the residual stress and Young's modulus for circular, square, and rectangular diaphragms [16]:

$$P = \frac{t}{a^2} W_0 \left[C_1 \sigma_0 + \frac{f(\nu)}{a^2} \frac{E}{1-\nu} W_0^2 \right] \quad (1),$$

where σ_0 = residual stress; P = pressure; t= film thickness; 2a = diaphragm width or diameter; W_0 = maximum center deflection; C_1= constant; v = Poisson's ratio; and f (ν) = function of Poisson's ratio[16].

The bulge test is a potentially powerful tool for characterizing thin film mechanical properties but is not utilized that much because of its sensitivity to experimental error and tedious sample preparation.

2.1.2 Micro-Beam Bending

In a bending test the force required to deflect the beam is much smaller than the force required for a tensile test or an indentation test. In a tensile test the force does not result in a visible displacement, whereas in bending the same force yields a displacement that is large enough to be measured optically (e.g. laser interferometer) or mechanically (e.g.

surface profilometer or nanoindenter) [17]. Microbeam deflection tests have been used to investigate thin film elastic modulus, and yield stress of the beam material. Microbeam deflection tests are done by a nanoindenter using its load and displacement monitoring system. By applying the basic theory of beam deflection one can determine the Young's modulus and yield stress. This method can be applied to free-standing films as well as to films on substrates [15].

Bilayer beams consisting of a substrate and a thin film are fabricated using conventional deposition techniques. The films are then patterned using standard photolithography processes, followed by anisotropic etching, rinsing, and drying. The final structures consist of cantilever beams extending over an open trench. Beam deflection can be performed by various methods. The most common method for beam deflection measurements is commercial load and depth-sensing indentation instrument capable of precise positioning of indentations.

Figure 2.3, shows a cantilever beam of length L with a point load F at its end. The deflection of the cantilever beam is:

$$Y_{\max} = \frac{FL^3}{3E^*I} \quad (2),$$

where F is the applied force, L the length of the cantilever, $I = wt^3/12$ is the relevant second moment of inertia of the beam, w the beam width, t the beam thickness. $E^* = E\varphi$, where φ is the anticlastic (saddle-like) correction factor. $\varphi = 1$ when the beam is long enough, and the plane-strain conditions along the beam width apply. This is the basic

bending mechanism used in simple beam deflection devices to obtain the Young's modulus.

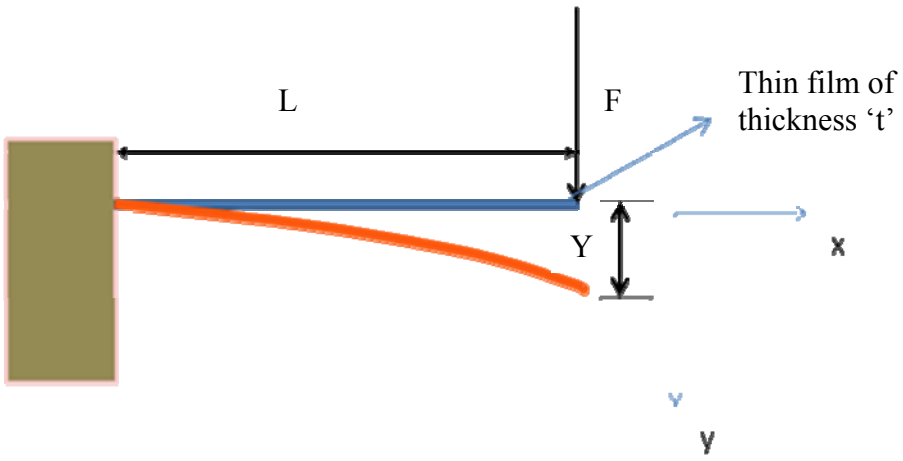

Figure 2.3. Simple Beam Deflection Schematic

The equation (2) is only valid to extract the ideal Young's modulus of the beam. However, some other effects such as undercut and anticlastic effects add some additional terms to equation (2). In this case the beam length, L, is replaced by $(L + L_C)$ in equation (2), where L_C is the required length correction. Thus we get an effective Young's modulus by replacing L in equation (2) with the corrected length.

2.1.3 Micro Tensile Test

The tensile test is the most efficient method because it directly measures elastic modulus, fracture strength and Poisson's ratio [18]. A simple schematic of the micro tensile testing

machine is shown in Figure 2.4. This experimental setup was used by K.M. Jackson *et. al.* [19] and W.N. Sharpe Jr. *et. al.* [20] to measure the mechanical properties of thin films. The specimen was placed in the grips, aligned and fixed in place with an ultraviolet cured adhesive. The specimen was elongated with a piezoelectric actuator until it failed, and then the strain was measured with a laser-based direct strain measurement device called the interferometric strain displacement gage (ISDG) [21].

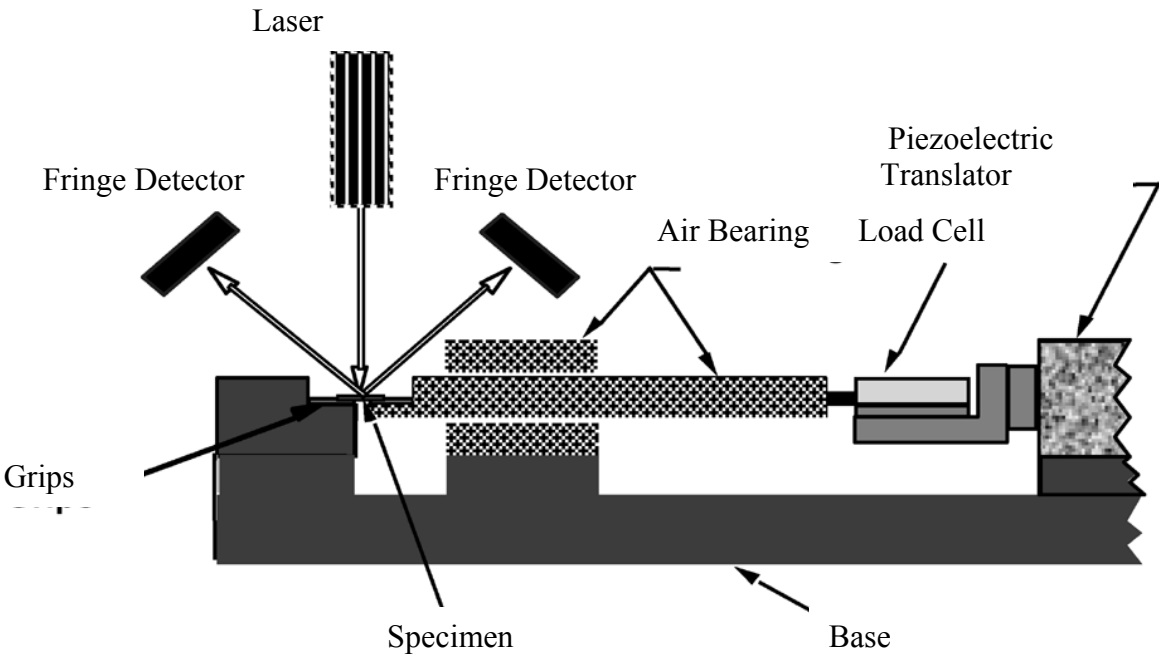

Figure 2.4. Schematic of Micro Tensile Testing Machine

This system worked extremely well for polycrystalline silicon and several other materials. But this system was not used for SiC because the difficulty in fabricating similar specimens created a greater challenge. Ironically, the same characteristics that make thin-film silicon carbide a viable alternative to polycrystalline silicon also make it a

difficult material to fabricate using conventional microfabrication tools. Micromolding was used to fabricate the SiC specimen in this case [19].

2.1.4 Scratch Test

Scratch testing is a combination of two operations: a vertical indentation motion and a horizontal dragging motion. In scratch testing the tip is dragged horizontally while simultaneously the load is increased in the vertical direction, which leaves a scratch mark on the thin film. This process may also detach the thin film from the substrate. Figure 2.5, shows how the system works based on the three plate capacitor system. The Triboindenter has sub-nanometer depth resolution due to its highly sensitive three plate capacitive transducer. The tip displacement and load are measured by a three plate capacitance system as shown in Figure 2.5. The piezoelectric scanner provides precisely controlled X, Y, and Z indenter tip position. The piezoelectric scanner moves the tip over a specimen, while a feedback loop controls the Z-axis height of the scanner to maintain a constant force between the indenter tip and the specimen. The Z-axis movement of the scanner is then calibrated to obtain a three dimensional topographical image [23]. This technique is used to either do indentation or scratch on the specimen.

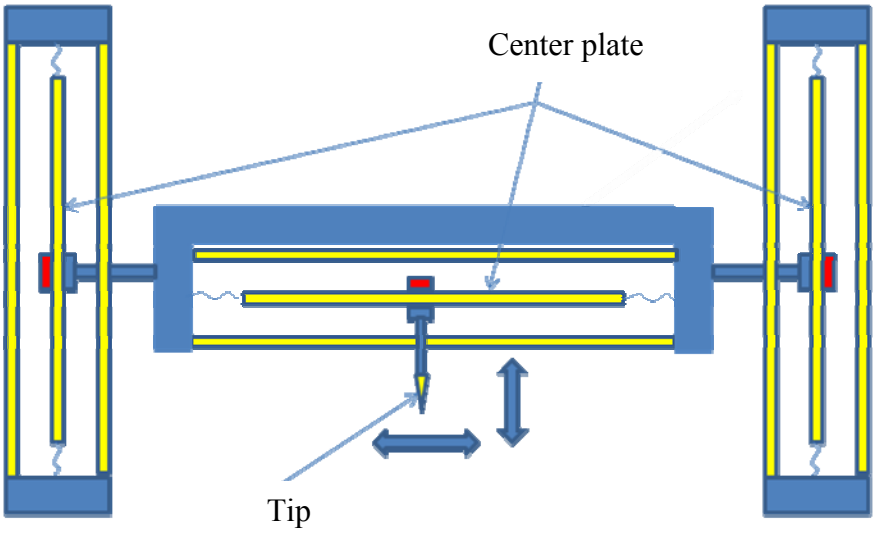

Figure 2.5. Hysitron Three Plate Capacitor Transducer

Hardness of the thin film can be calculated by measuring the scratch width ***b,*** shown in Figure 2.6. The scratch morphology on a gold film can be seen in Figure 2.6. This width ***b*** is used in equation 3 to determine the hardness of the material:

$$H = \frac{8F_N}{\pi b^2} \quad (3),$$

where F_N is the normal applied load and ***b*** is the scratch track width.

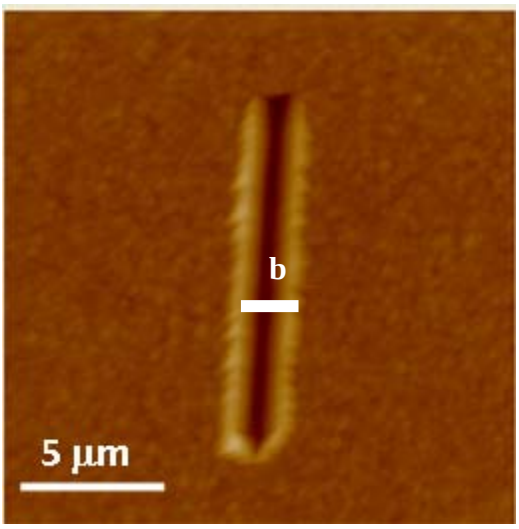

Figure 2.6. Scratch Morphology on Gold Film

The critical normal load measured is used to calculate the practical work of adhesion of the film to the substrate [13]:

$$P_{Cr} = \frac{\pi r^2}{2}\left(\frac{2EW_{A,P}}{h}\right)^{\frac{1}{2}} \quad (4),$$

where r is the contact radius, E is the elastic modulus of the film, $W_{A,\,P}$ is the practical work of adhesion and h is the film thickness. Equation (4) applies only when the thin film delaminates due to normal applied force, and does not account for the residual stress in the thin film.

2.1.5 Nanoindentation

There are various methods used as mentioned in the above sections to determine the mechanical properties of thin films. Bulge test, micro-beam bending, micro tensile test [2], nanoindentation, etc., are a few methods used to determine the mechanical properties

for the thin films. Nanoindentation is widely accepted method used to determine the mechanical properties of thin films.

Nanoindentation is a very successful way for measuring the elastic modulus and hardness of thin films [22], the goal of the majority of nanoindentation tests is to determine the elastic modulus and hardness from load-displacement measurements [23]. However, it can also be used to measure thin film adhesion, and fracture toughness.

General hardness testing machines allow measuring the size of the residual plastic impression on the specimen as a function of the indenter load. This gives the area of the residual imprint for an applied load; which is on the order of few square microns, and can be measured using optical techniques. In the nanoindentation method, the tip penetration depth is measured as the load is applied to the indenter. Knowing the geometry of the indenter allows the size of the area of contact to be determined. The depth of the impression is on the order of tens of nanometers. The modulus of the material can be obtained from the measurement of the unloading stiffness i.e., the rate of change of load and depth.

The advantage of nanoindentation over other methods is that it is a relatively simple and direct method. Nanoindentation is the process in which a sharp indenter is forced in to the sample of interest and withdrawn. Figure 2.7, gives the schematic of the Nanoindenter used for testing the mechanical properties of thin films.

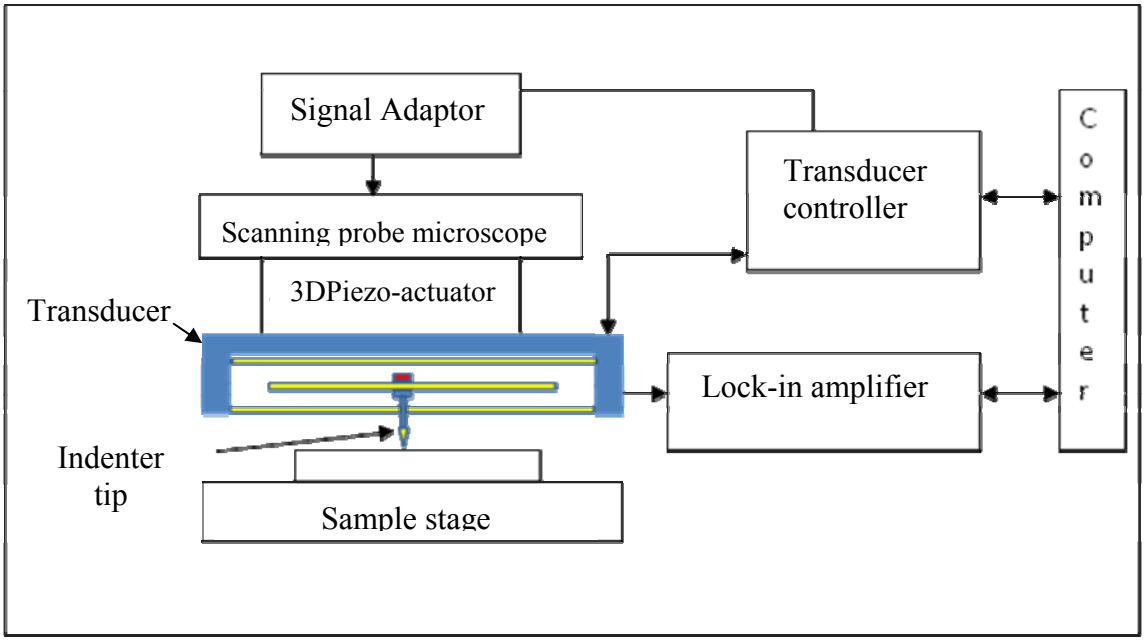

Figure 2.7. Schematic of the Nanoindenter (Triboindenter)

In nanoindentation, depth sensing techniques are used where the modulus of the specimen is obtained from the slope of the initial unloading portion of the load-displacement curve. The modulus obtained from the sample is defined as reduced, contact, or indentation modulus. Nanoindentation and measurement of mechanical properties of thin films using Nanoindentation is further explained in detail, in Chapter 3.

CHAPTER 3

3.1 Nanoindentation

This chapter provides a brief introduction to the Hysitron Triboindenter, and various applications of nanoindentation measurements, including hardness, Young's modulus and other mechanical properties.

3.1.1 Hysitron Triboindenter

The Triboindenter is one of the most advanced machines for testing mechanical properties; it is a fully automated multi-load range indentation/scratch testing system designed for measuring hardness, elastic modulus and dynamic viscoelastic properties of thin films. The Hysitron Triboindenter was developed to operate in quasi-static or dynamic loading modes and has optional acoustic emission testing capabilities. The most distinguishing feature of Triboindenter is it has a low noise floor, making it possible to do shallow indentations of the order of 10 nm or less and piezoelectric topography in-situ scanning of pre and post indentation features on the specimen surface.

This high-performance staging system showed in Figure 3.1 offers superior stability and flexibility to accommodate a wide range of applications, sample sizes and types. It uses a patented transducer shown in Figure 2.5. This transducer is the heart of the Hysitron

indenter, the force applied is an electrostatic force while the displacement is measured by the change in capacitance. This electrostatic actuation does not use much current, which makes it virtually drift-free due to low heating during actuation.

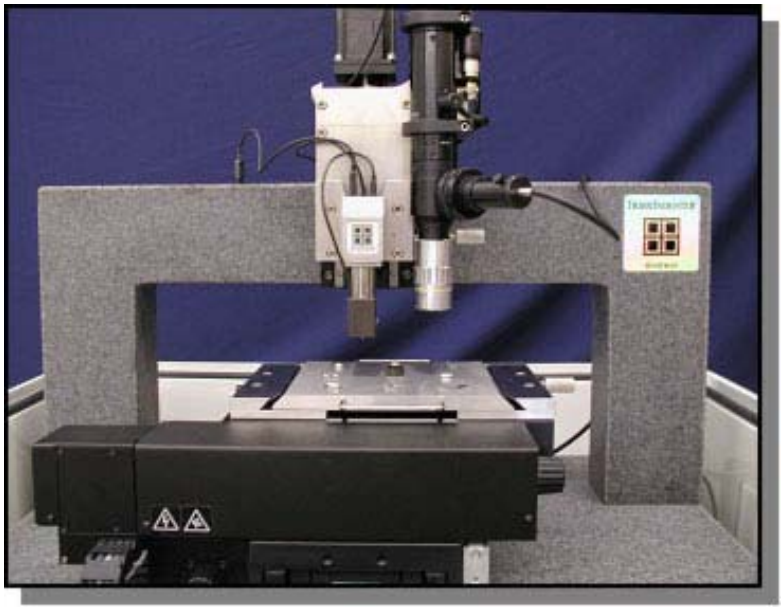

Figure 3.1. Triboindenter Main Unit (Hysitron Inc)

This patented three-plate capacitor technology provides simultaneous actuation and measurement of force and displacement [24]. The Triboindenter can be operated in both open loop or closed loop displacement or force control modes. This means that the user chooses the mode of operation and amount of force or displacement that will be applied by the indenter [25]. Hysitron comes with a high load module which can perform indentations up to a load of 2 N.

3.2 Testing of Thin Films

Elastic modulus E, and hardness, H are the thin films properties most frequently measured in a nanoindentation experiment. Through nanoindentation one can obtain both qualitative and quantitative data from a thin film system. The major misinterpretation of data in nanoindentation arises when the tip indenter unintentionally probes the substrate. In order to avoid this misinterpretation, the maximum depth of penetration has to be restricted to 10% of the film thickness [26]. Some of the important factors that need to be taken care of while using nanoindentation are described in the following paragraphs.

3.2.1 Tip Geometry

In this thesis experiments were performed using Berkovich indenter tip. It has a face angle of $\theta = 65.27°$, which has the same projected area-to-depth ratio as the Vickers indenter. However, the original Berkovich indenter had a different angle of 65.03, although it gives the same actual area-to-depth ratio as the Vickers indenter as well [27]. For a Berkovich indenter the projected contact area A is given by equations (6) and (7):

$$A = 3\sqrt{3}h_c^2 \tan^2 65.27^\circ \quad (6),$$

$$A = 24.5h_c^2 \quad (7),$$

where h_c is the contact depth. Figure 3.3 gives the profile of the film surface before and after indentation. All values obtained from a quasi-static nanoindentation analysis depend

on accurate knowledge of the shape of the indenter tip. Thus the tip shape function $A(h_c)$ must be determined.

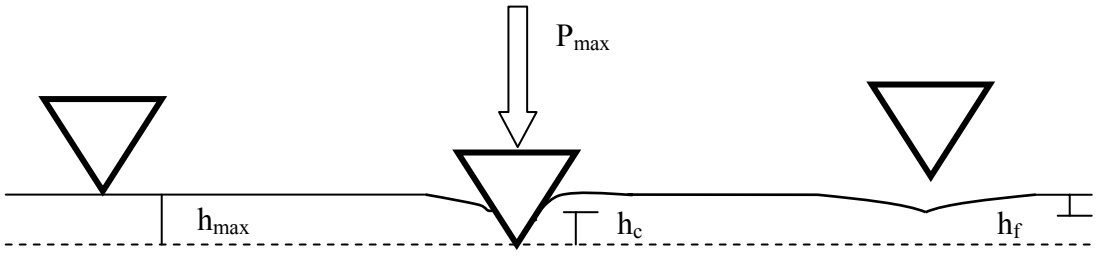

Figure 3.2. Profile of the Film Surface Before and After Indentation

In nanoindentation, the contact area at h_c is not accurate or may be valid only for the ideal geometry of the indenter tip. In reality the tip geometry varies, so in order to get reliable data one needs to obtain the tip area function which takes into consideration the true shape of the indenter tip. This is explained in the following paragraphs.

3.2.2 Tip Shape Function

There are various methods used to find the tip shape function. The most precise but impractical way is by measuring the residual contact area in the Transmission Emission Microscope using the replica method. Other methods are to image the tip of the indenter with a scanning force microscope (SFM). However, in this case the tip shape of the SFM must be accurately known to assess the final shape of the tip which is being imaged. The most prevalent and practical solution to find out the tip shape is by carrying out indentations on various materials with known elastic properties. An iterative procedure is

used to find the compliance of the machine and the tip area function [28]. In this case the experimental data are often fitted using equation (8):

$$A(h_c) = C_0 h_c^2 + C_1 h_c + C_2 h_c^{\frac{1}{2}} + C_3 h_c^{\frac{1}{4}} + C_4 h_c^{\frac{1}{8}} + C_5 h_c^{\frac{1}{16}} \quad (8),$$

In case of an ideal Berkovich diamond indenter C_0 should be set to 24.5. In general it is preferable to use as few coefficients as possible. To calculate both the elastic modulus and hardness the projected contact area is required. At large contact depths the ideal tip area function, mentioned in equation (7) can yield accurate results, whereas at low contact depths the actual tip geometry must be taken into account to get accurate results.

Since the indents are small, the area of the indent cannot be measured directly, or by optical microscopy. In order to find the contact area, a number of indents are made in samples with known elastic properties. This contact area is then calculated from the empirical formula, $A = f(h_c)$, which relates the projected contact area (A) is a function of the contact depth (h_c).

To determine the tip area function of the indenter tip, multiple indents are made in (100) silicon which has the elastic modulus of 174 GPa. Figure 3.3 shows contact area variation with the contact depths. Figure 3.4, shows us the plot between contact depth and 0contact area.

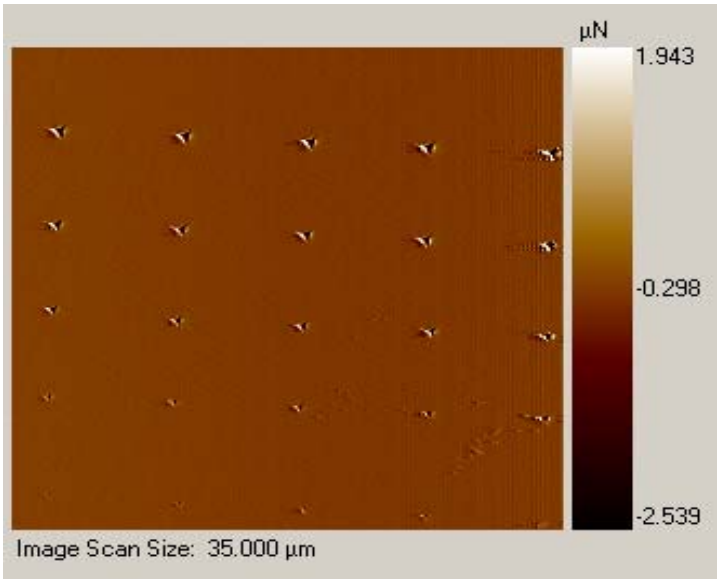

Figure 3.3. Topographic Image at Various Contact Depths

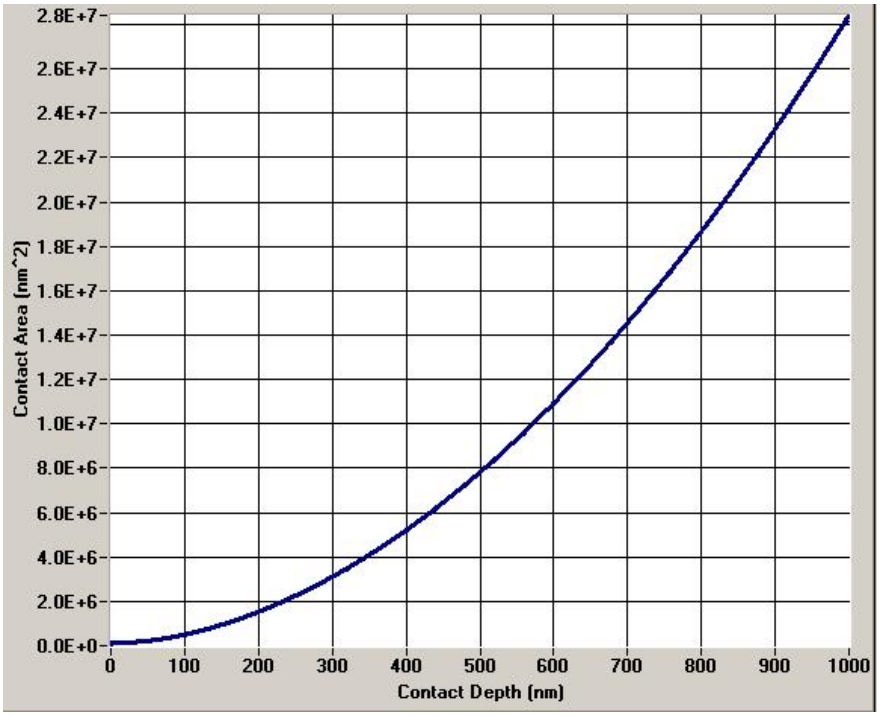

Figure 3.4. Contact Area Plot With Respect to the Contact Depth of the Tip

Figure 3.5 shows the plots obtained for the load-displacement curves for Si (100) performed at different loads. The residual impressions of the indenter on the silicon

surface can be seen in Figure 3.4. In this procedure, 25 indentations were made starting from 400 μN maximum load to 10 mN load with an increment of 400 μN to have the full range of required displacements. From the known values of Si properties, one can relate contact depths to contact area of the tip for various depths from the empirical fit of equation (8). This area function is used to determine hardness and elastic modulus for unknown materials.

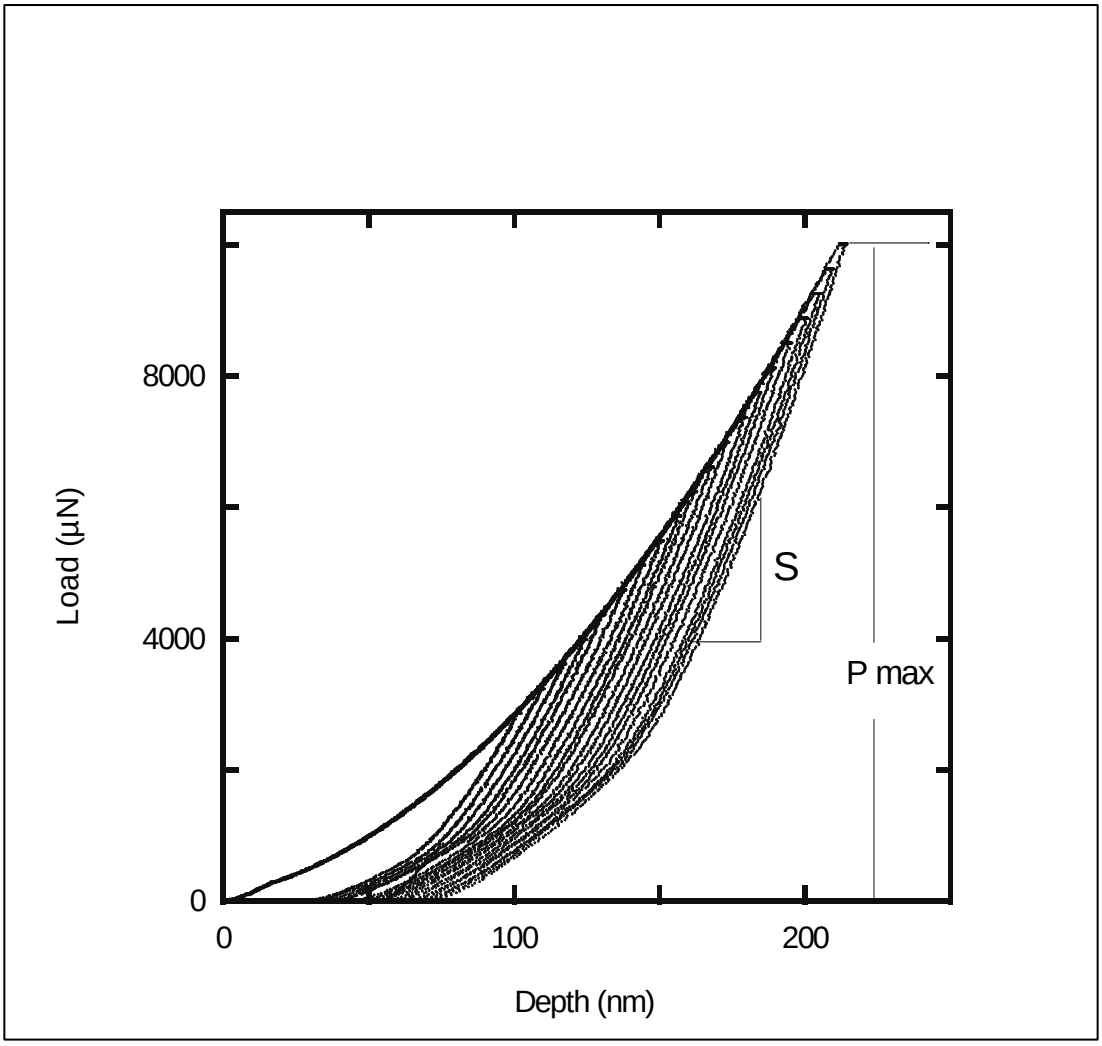

Figure 3.5. Multiple Load-Displacement Curves Obtained From Indenting (100) Si

3.3 Measurement of Elastic Modulus

The most common method for measuring hardness and modulus using nanoindentation methods involves making a small indentation in the film, while continuously recording the indentation load, P, and displacement h, during one complete cycle of loading and unloading. Stiffness of the contact between the indenter and the material being tested is required to determine the mechanical properties of interest. The stiffness, S, is determined from the initial slope of the unloading curve. $S = dP/dh$, where P is described by the power relation given by Oliver and Pharr [22]:

$$P = A(\delta - \delta_{pl})^m \quad (9),$$

where A and m are fitting parameters, P and δ are the load and displacement taken from the top 65% of the unloading curve. The loading and unloading portion can be seen in Figure 3.6

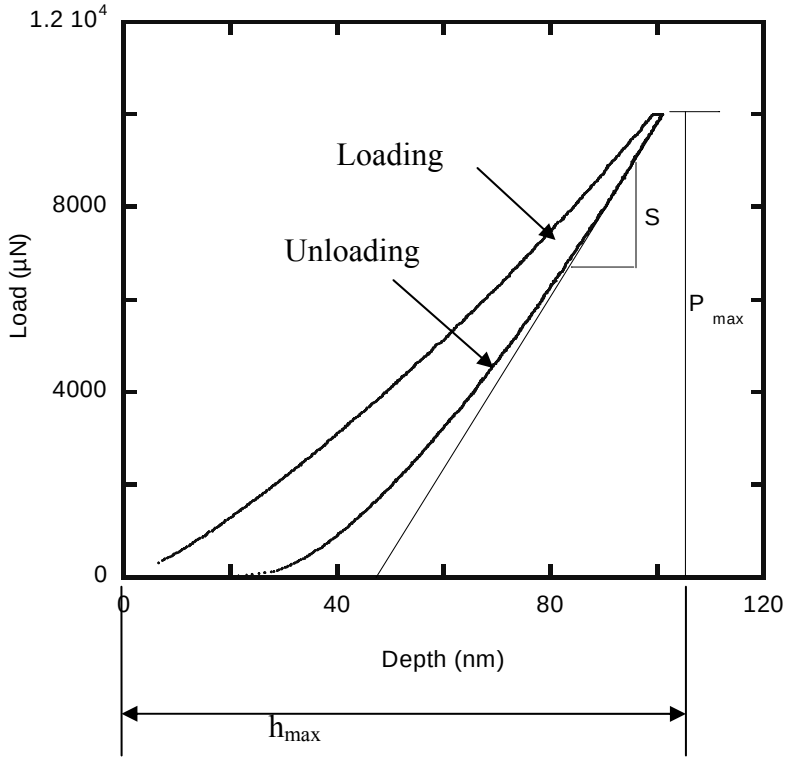

Figure 3.6. Schematic of Load-Displacement Curve for Depth Sensing Indentation Experiment

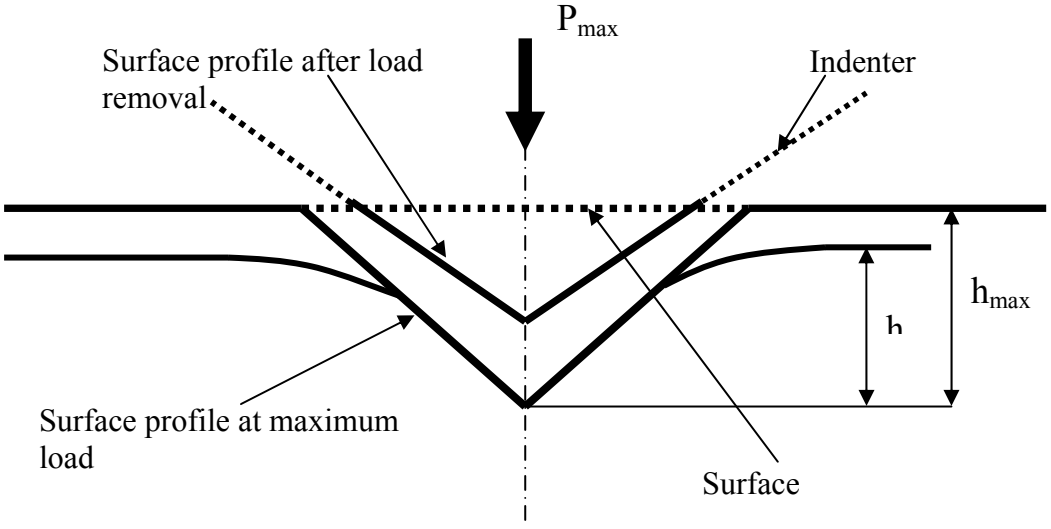

Figure 3.7. Schematic of Indentation Cross-Section Showing Various Parameters

Various indent parameters are shown in Figure 3.7. The indent cross-section explains the residual imprint of the indent after unloading. One can also observe the elastic recovery, which gives a clear picture of surface profile at the maximum load. Once the stiffness is measured using equation S = dP/dh, the reduced modulus can be determined as:

$$E_r = \frac{\sqrt{\pi}}{2}\frac{S}{\sqrt{A}} \quad (10),$$

where E_r is the reduced modulus, which accounts for the measured elastic displacement contributing from both the sample and the indenter tip. The reduced modulus can be used to calculate the actual modulus of the sample, which is given by:

$$\frac{1}{E_r} = \frac{1-\nu_{sample}^2}{E_{sample}} + \frac{1-\nu_{tip}^2}{E_{Tip}} \quad (11),$$

where E_{tip} = 1140 GPa and V_{tip} = 0.07 are the elastic modulus and Poisson's ratio for diamond tip, respectively. From this equation we can calculate the E_{sample} for the given sample.

3.4 Hardness

Hardness is the resistance to the plastic deformation and it is given by:

$$H = \frac{P_{max}}{A} \quad (12),$$

where P_{max} is the maximum load and A is the projected area of contact or hardness impression. The effect of indentation depth on hardness measurement has been a real area

of concern. When low loads are applied the resultant area of contact might be very small or sometimes it recovers elastically with no residual impression left behind. This gives an exaggerated hardness value. The most common method to determine the hardness of a material is by static indentation. Hardness can also be determined using scratch hardness testing using the same nanoindentation machine. This method is explained in detail in section 2.1.4.

Precautions should be taken in order to avoid discrepancies in calculating mechanical properties from nanoindentation data. Indents should not be made too deep into the thin film as the substrate effects may be noticed [29]. In an attempt to avoid substrate effect on thin film elastic modulus and hardness, often excessively shallow indents are made into the thin film. By taking indents that are not deep enough, the elastic modulus and hardness measurements will be inaccurate. This inaccuracy is due to surface roughness, possible oxidation effects and errors in assessing the tip contact area [30].

3.5 Fracture Toughness

Since a nanoindenter is a versatile machine it can be used to evaluate the fracture toughness of a given bulk material. Small cracks on the surface of thin films can be induced when higher loads are applied. These patterns of cracks are used to assess the film fracture toughness. Cracks come in different morphology depending on the indentation load, tip indenter geometry and material properties. The most common kind of cracks are radial cracks for brittle and hard materials [31, 32]. Figure 3.8, shows the schematic of load-induced radial cracks propagating from indentation using a Berkovich

tip. Fracture toughness is calculated from equation (13), this is the most widely used relationship [31]:

$$K_c = A\left(\frac{E}{H}\right)^{\frac{1}{2}} \frac{P}{C^{3/2}} \qquad (13),$$

where, K_c is the fracture toughness, P is the maximum load, C is the crack length, E is the elastic modulus and H is the hardness, A is an empirical constant, for the Berkovich tip it is 0.016[23].

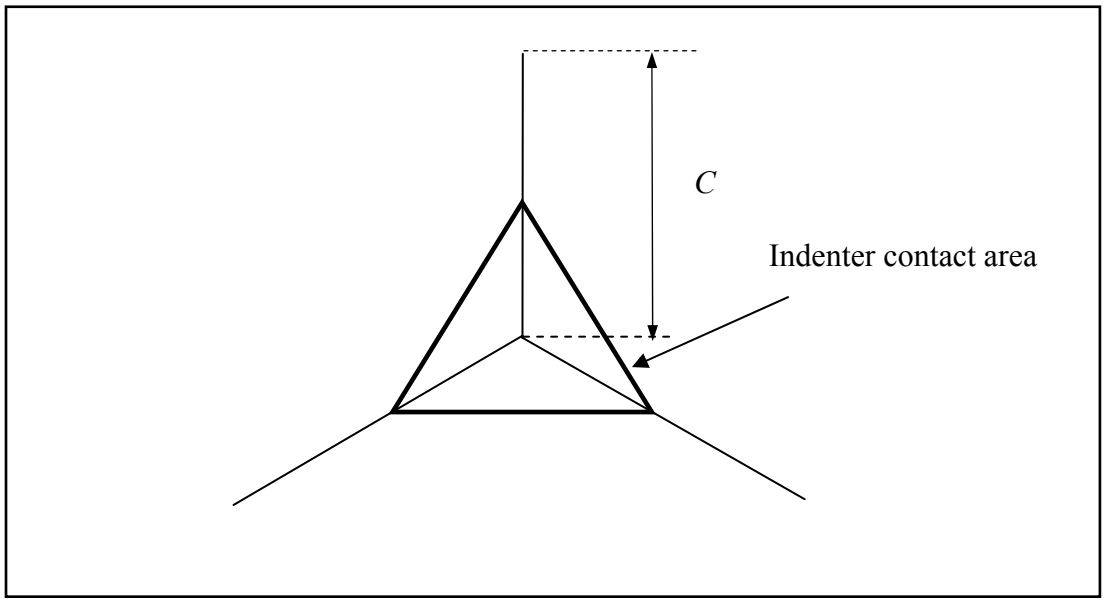

Figure 3.8. Schematic of the Radial Cracks Induced by Berkovich Indenter

Generally there are three types of cracks, radial cracks, lateral cracks, and median cracks. Radial cracks occur on the surface of the specimen at the corners of the indenter edge marks. These cracks are generally formed due to the hoop stress. Figure 3.8, shows a schematic of radial crack propagation at the edges of the indenter contact site. Lateral

cracks are cracks which occur beneath the surface. These cracks are generated by tensile stress and often extended to the sample surface. Median cracks are circular penny shaped cracks that are formed beneath the surface and along the line of symmetry. Fracture mechanics treatment of these types of radial and lateral cracks is useful to provide the fracture toughness based on the length of radial cracks [33].

3.6 Hertzian Contact Theory

In nanoindentation the most predominantly used indenter tip is the Berkovich tip, which has the shape of a three-sided pyramid. Berkovich indenters are not perfectly sharp. The most common assumption is to describe the Berkovich indenter as spherical at its tip [34]. However, since the radius R of the tip is not known, most users use the tip radius specified by the manufacturer [35]. These assumptions are subjected to great uncertainty since the indenters can wear out and change their tip geometry. To avoid such errors some researchers have directly measured the tip radius by scanning the tip using atomic force microscopy or by scanning electron microscopy [36].

Another popular approach to determine the radius of the tip is to fit the load-displacement curve with the Hertzian equation. The stresses and deflection arising from the contact between two elastic bodies are of particular interest for indentation testing. Hertz found that the radius of the circle of contact ‘a’ is related to the indenter load P, the indenter radius R, and the elastic properties of contacting materials by equations (14) and (15): Hertz originally derived the equation for two cylinders in contact; this theory is applied to the spheres in this case.

$$a^3 = \frac{3}{4}\frac{PR}{E_r} \tag{14},$$

$$P = \frac{4}{3}E_r R^{\frac{1}{2}} h^{\frac{3}{2}} \tag{15},$$

where P is the indenter load, h is the displacement, and E_r is the reduced modulus, [37] which can be determined from equation (11). Once the radius is known the stresses in the material can be evaluated from the Hertzian contact mechanics as a function of applied load. In this research we establish the tip radius using the Hertzian curve fit. Figure 3.10, gives the Hertzian fit for the loading curve of a thin film sample which was indented using the Berkovich tip.

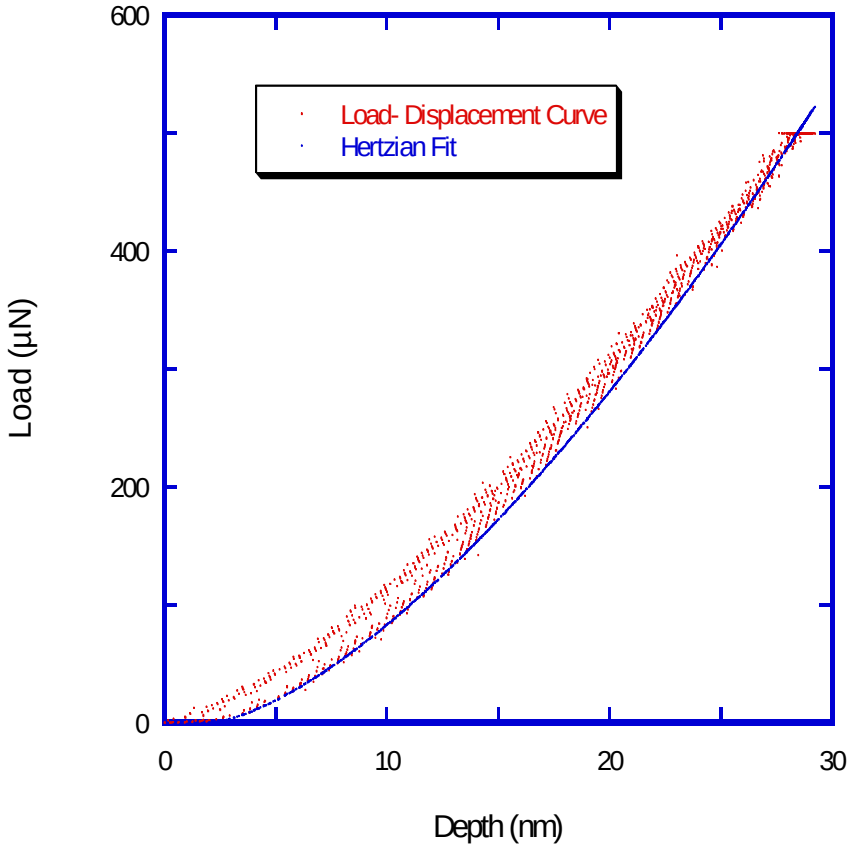

Figure 3.9. Comparison of Elastic Load-Displacement Data and the Hertzian Curve Fit

This Hertzian curve fit was obtained from indentitions made in the SiC thin films. To find the radius of the tip, experiments were done at low loads up to 500 µN to obtain complete elastic load-displacement curves as shown in Figure 3.10.

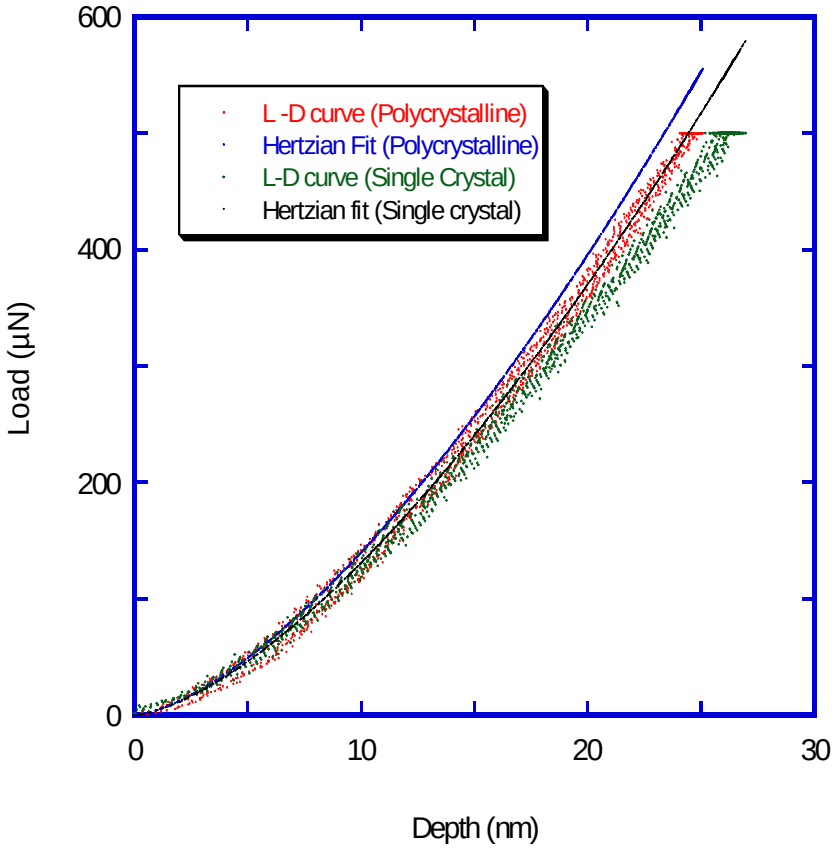

Figure 3.10. Elastic Load-Displacement and the Hertzian Curves Obtained From SiC Thin Films

From Figure 3.11, one can observe that the Hertzian curve fit was done on both single crystal and polycrystalline SiC elastic load-displacement curves to extract the radius of the Berkovich indenter. The radius of the tip was found to be approximately 100 – 110 nm. This indenter tip is used in the experiments done, which is explained in chapter 4.

CHAPTER 4

4.1 Mechanical Characterization of SiC Using Nanoindentation

This chapter deals with growth of single crystal and polycrystalline SiC and experiments performed on the single crystal SiC, polycrystalline SiC, bulk SiC (Lely Platelet SiC), and bulk Si (100) films using Hysitron Triboindenter. This chapter talks about sample preparation, experimental setup and the obtained results.

4.1.1 Sample Preparation

Two samples were studied and their mechanical properties such as elastic modulus, hardness and fracture toughness were compared. The samples used for the comparative study were single crystal 3C-SiC and polycrystalline SiC, grown by heteroepitaxy chemical vapor deposition. Film thickness of the samples were around 1-2 μm.

4.1.2 Growth of Single Crystal 3C-SiC Films

The most common technique used to grow crystalline films epitaxially is CVD. 3C-SiC single crystal films were grown on 50-mm diameter (100) Si wafers using hot-wall CVD. The design of the CVD reactor can be found elsewhere [38]. The 3C-SiC on Si growth process was developed using the two step carbonization

and growth method. C_3H_8 and SiH_4 were used as the precursor gases to provide the carbon and silicon sources, respectively. Ultra high purity (UHP) hydrogen, purified in a palladium diffusion cell, was employed as the carrier gas. Prior to growth, the samples were prepared using the standard RCA cleaning method [39], followed by a 30 second immersion in diluted hydrofluoric acid (HF), to remove surface contaminants and native oxide. The first stage of the process, known as the carbonization step, involved heating the reactor from room temperature to 1140 °C at atmospheric pressure with a gas flow of 6 standard cubic centimeters per minute (sccm) of C_3H_8 and 10 standard liters per minute (slm) of H_2. The temperature was then maintained at 1140 °C for two minutes to carbonize the Si substrate surface. After carbonization, SiH_4 was introduced into the system at 4 sccm and the temperature increased to growth temperature of 1375 ºC, and gas pressure of 100 Torr was maintained for approximately 5 minutes. The temperature and other flow rates were maintained constant during the growth process. By this procedure, a sample 2 μm thick 3C-SiC was grown.

After the growth process was completed, the wafer was cooled to room temperature in Ar atmosphere [13]. After deposition the film thickness was measured by Fourier Transform infrared transform (FTIR) and confirmed by scanning electron microscopy. The crystal orientation of the film deposited was determined by X-ray diffraction (XRD) using a Philips X-Pert X-ray diffractomer. XRD data proved that the films were single crystal. Figure 4.1, shows the rocking curve obtained from the (200) planes for 3C-SiC grown on (100) Si. This data confirms the film is single crystal 3C-SiC.

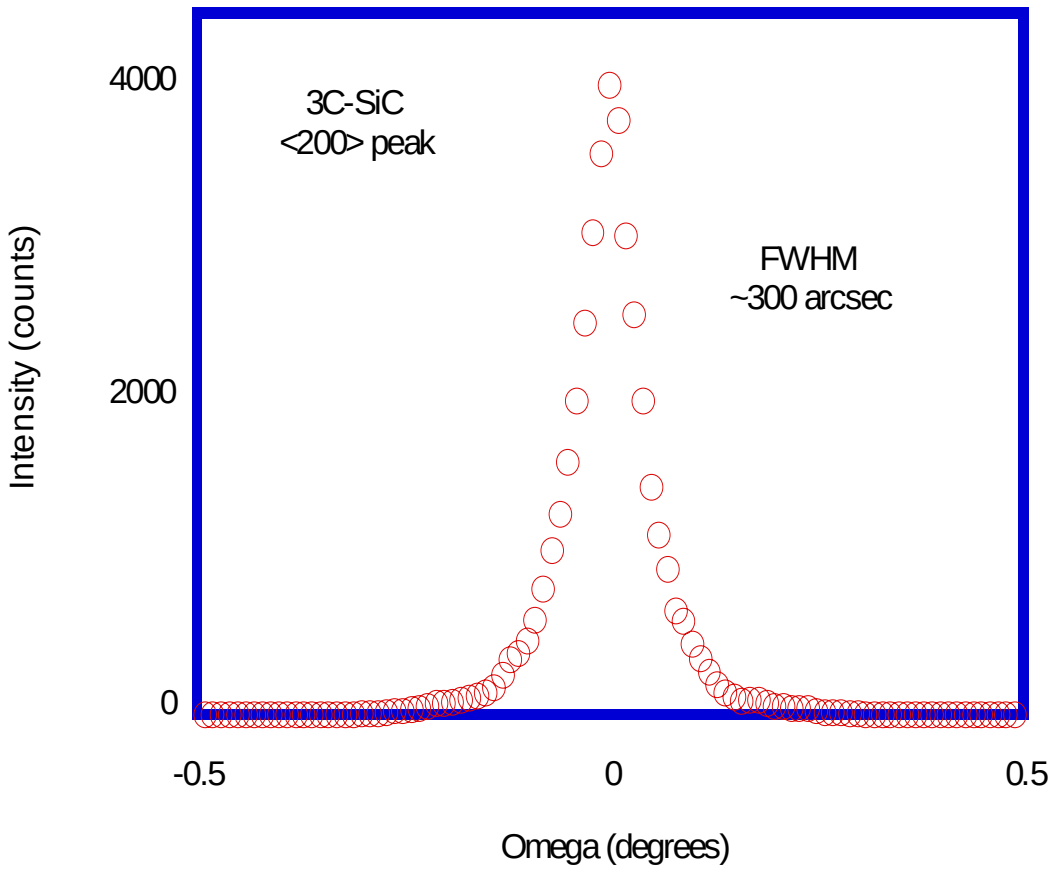

Figure 4.1. Rocking Curve From the (200) Planes of 3C-SiC Grown on Si (100)

4.1.3 Growth of Polycrystalline 3C-SiC Films

Polycrystalline growth follows the same procedure as single crystal SiC with the exception of a higher gasses flux. The process conditions for the samples studied here were identical to those listed above except that the SiH_4 and C_3H_8 mass flow rates were 6 sccm and 4 sccm, respectively. This process resulted in a polycrystalline-3C-SiC film.

4.2 Experiments and Results

This section explains the results obtained from the experiments conducted using the nanoindenter and the analysis of the data to determine the mechanical properties. Samples of same film thickness (2 μm) were used to conduct the experiments. The samples tested were 3C-SiC single crystal grown on Si (100). This sample had a good optical-quality-smooth-surface requiring no further polishing. On the other hand, the deposited polycrystalline sample was rough and needed mechanical polishing. The sample was polished using a 1 μm pad with Leco® diamond paste to smooth the film surface and reduce the film thickness to match the thickness of the single crystal SiC film (2 μm). These samples were then cleaved and glued to the sample holders using cyanoacrylate (Super glue).

The Berkovich indenter was used for all indentation tests. This is the best tip for most bulk samples, unless the RMS roughness is higher than 50 nm [25]. Load controlled indentations were performed to determine films elastic modulus and hardness.

4.2.1 Surface Polishing

Polycrystalline SiC was polished since its as-deposited surface was too rough, and indentation experiments were not giving matching load-displacement curves. Figure 4.2, shows the root mean square roughness, average roughness, and peak-to-valley height before polishing. Figure 4.3, is the 3D image of the as-deposited polycrystalline specimen before polishing. Figure 4.4, gives an insight as to why polycrystalline SiC had to be polished before doing experiments.

The uneven loading and unloading curves were observed on this specimen mainly because of the coarse surface where the tip slips between the peaks and the valleys of the film surface. This excessive surface roughness was giving unrepeatable results; in order to obtain repeatable loading and unloading curves the specimen was polished with 1 micron diamond paste. After polishing the topographic scans were taken and the indentation experiment was repeated for the same maximum loads.

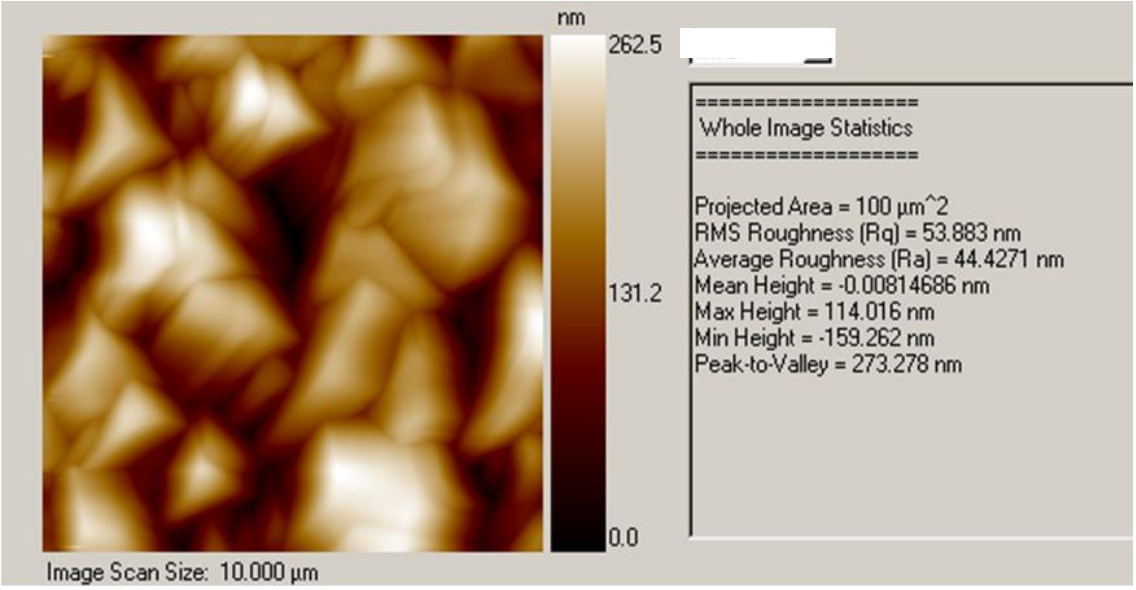

Figure 4.2. RMS Roughness and Average Roughness Values of the Unpolished SiC

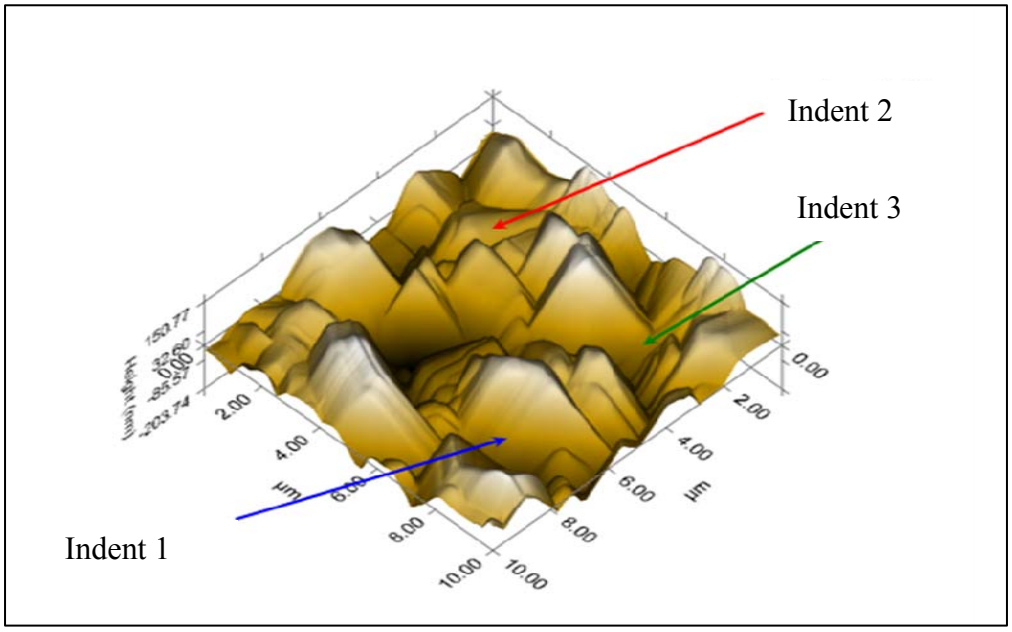

Figure 4.3. Topographic Image of the Polycrystalline SiC Before Polishing

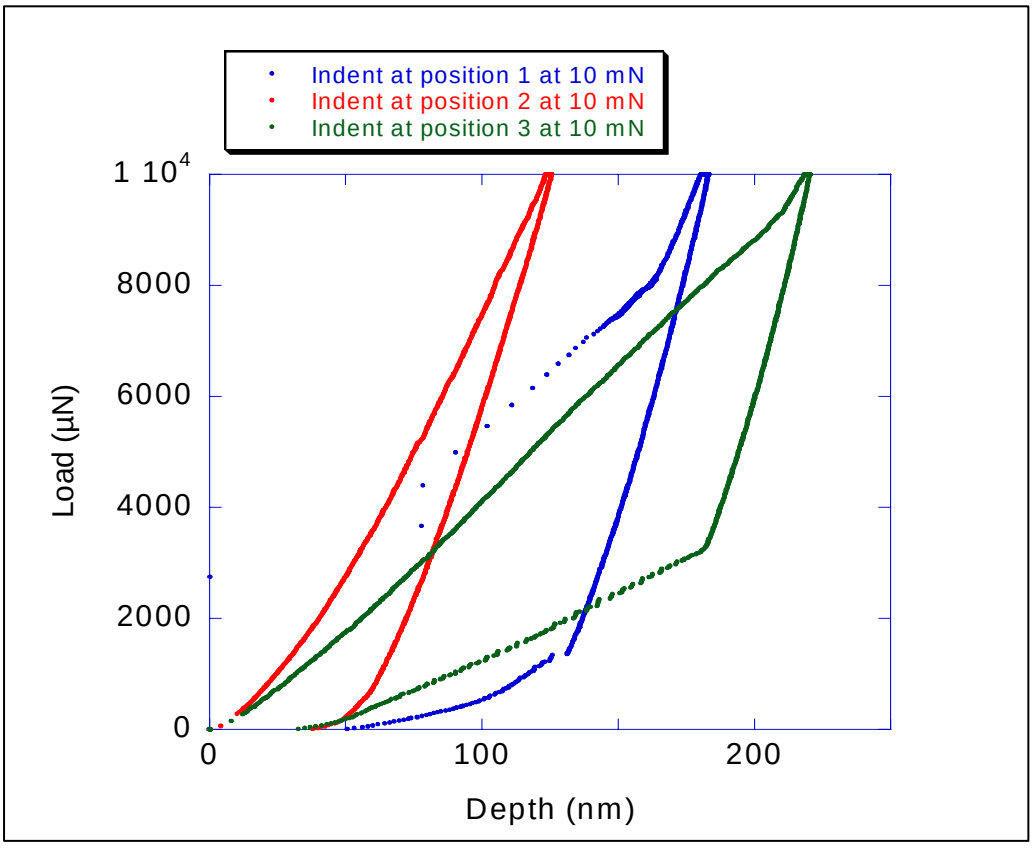

Figure 4.4. Load-Displacement Curves Before Polishing

Figure 4.5, gives the RMS roughness, average roughness, and peak-to-valley height of the polycrystalline SiC after polishing. Figure 4.6, is the topography image of the SiC after polishing and Figure 4.7, shows the load-displacement curves obtained after polishing. Before polishing the average roughness was 44.4 nm, and the RMS roughness was 53.9 nm. After polishing the average roughness was 1.5 nm, and RMS roughness was 2 nm.

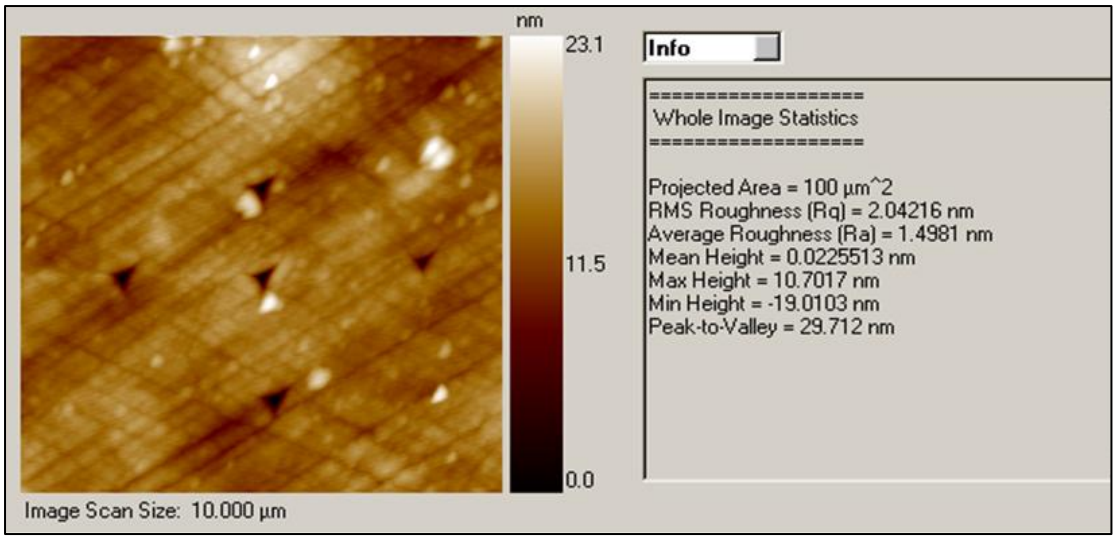

Figure 4.5. RMS Roughness and Average Roughness Values After Polishing Polycrystalline SiC

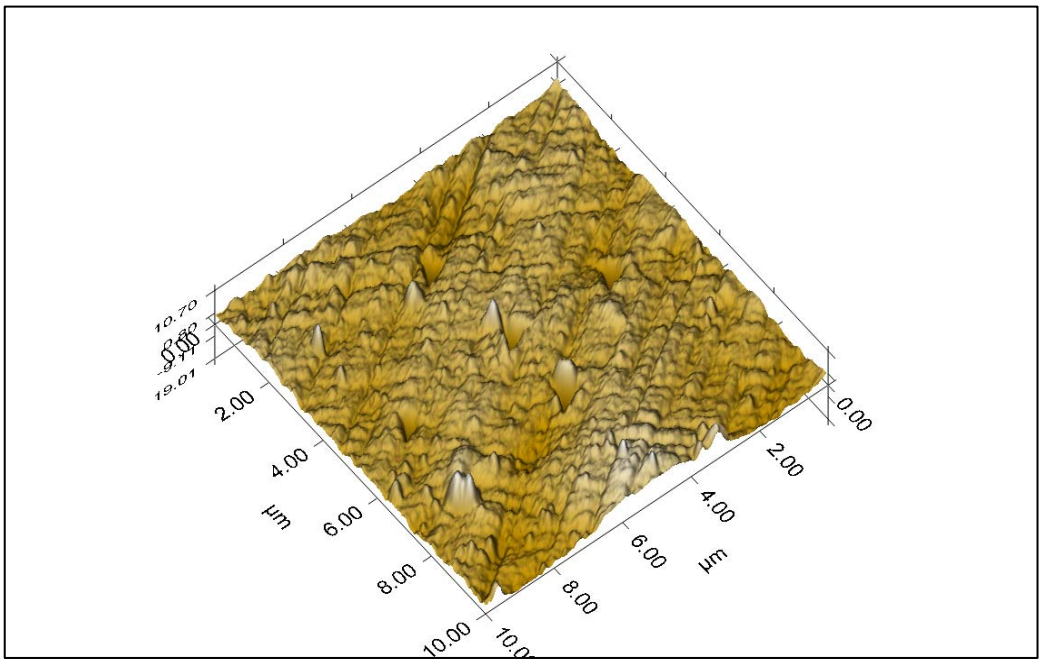

Figure 4.6. Topographic Image of the Polycrystalline SiC After Polishing

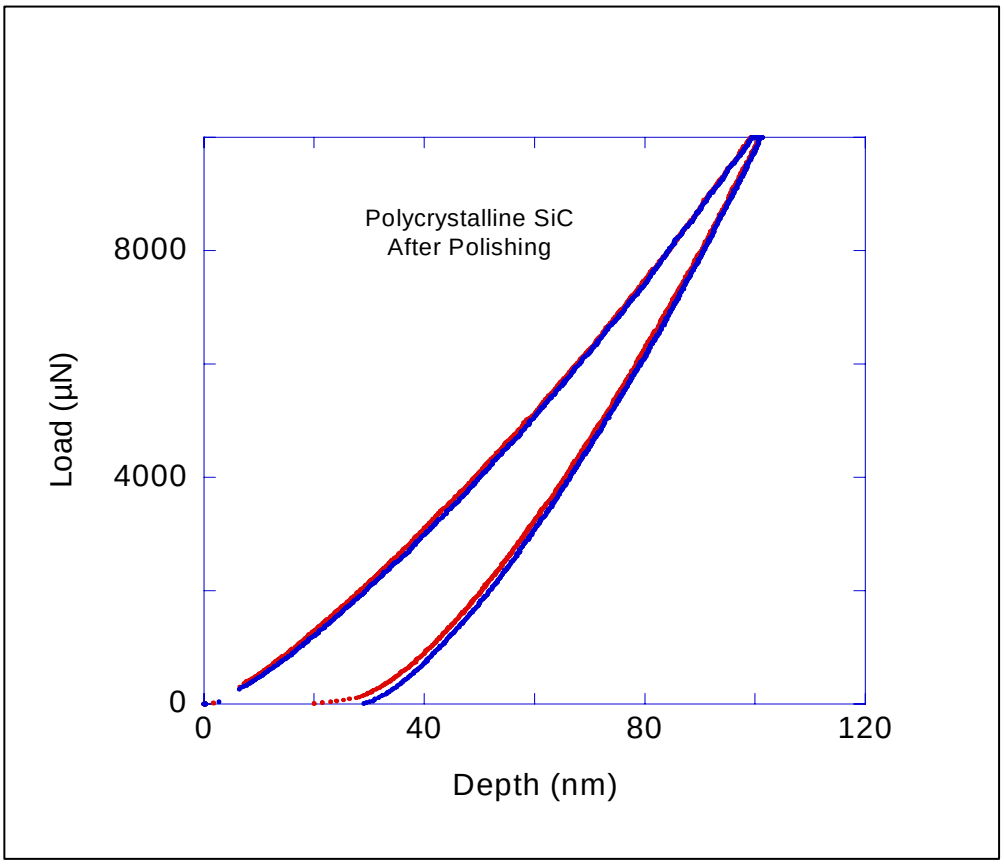

Figure 4.7. Load-Displacement Curves After Polishing Polycrystalline SiC

4.2.2 Analysis of Hardness and Elastic Modulus for SiC

Standard low load transducer, which can apply a maximum load of 10 mN, was used to find the elastic modulus (E) and hardness (H) of the deposited films. The experiment was carried at loads varying between 500 μN to 10 mN on both the single crystal and polycrystalline SiC samples. The load-displacement curves obtained from single and polycrystalline SiC films are compared in Figures 4.8 and 4.9. The hardest materials of the two has less penetration depth for the same load, hence polycrystalline SiC is harder.

From Figure 4.8, it can be inferred that at lower load both the single and polycrystalline samples exhibit similar elastic contact. Also elastic load-displacement curves helps in determining the radius of the indenter tip used in performing the nanoindentation experiments, by using the Hertz theory of elastic contact [16, 24]. Using high loads varying from 5mN to 10 mN we saw the plastic deformation in the film. Figure 4.10 shows the indentation done at a load of 10 mN, from which it can be inferred that the indenter penetrated more into the single crystal SiC than polycrystalline SiC.

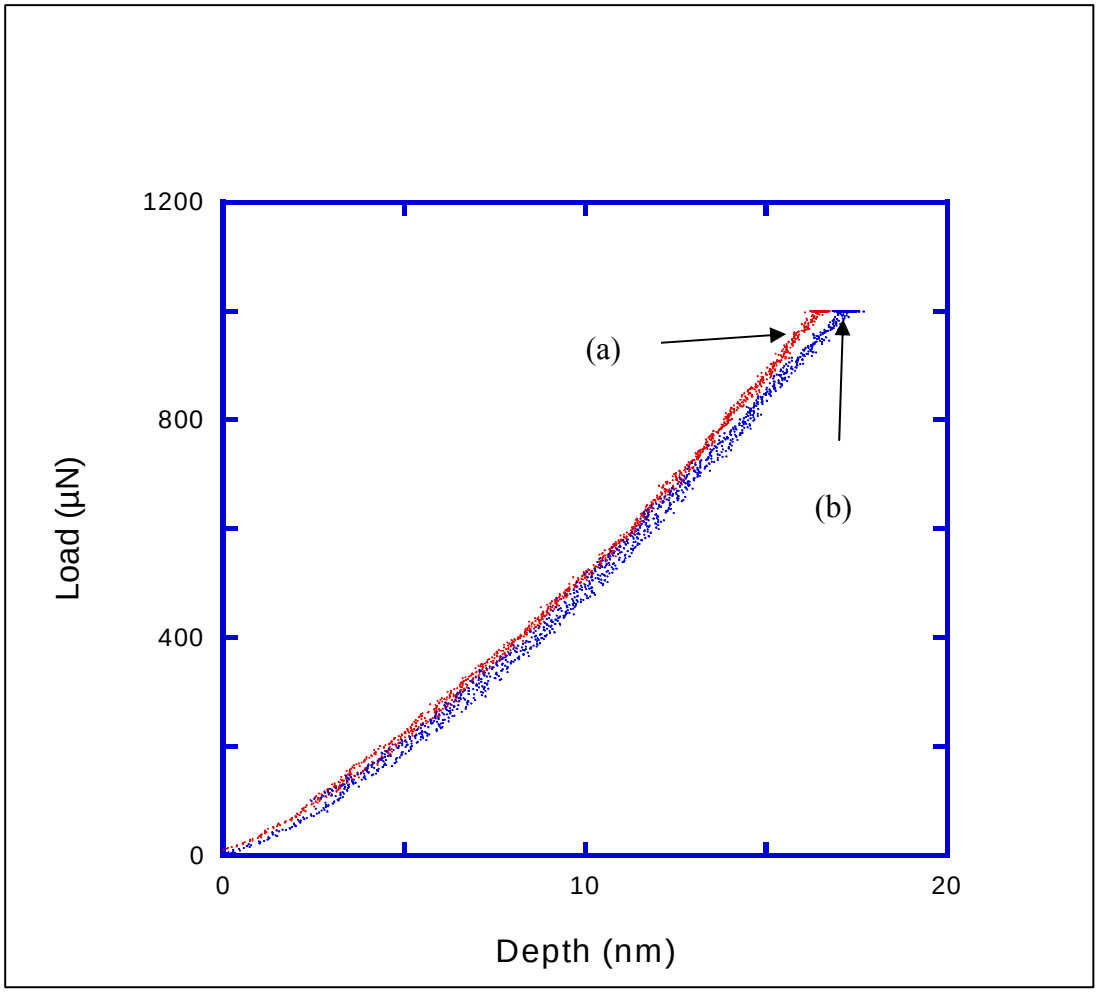

Figure 4.8. Load-Displacement Curve at a Load of 1 mN (a) Polycrystalline SiC (b) Single Crystal SiC

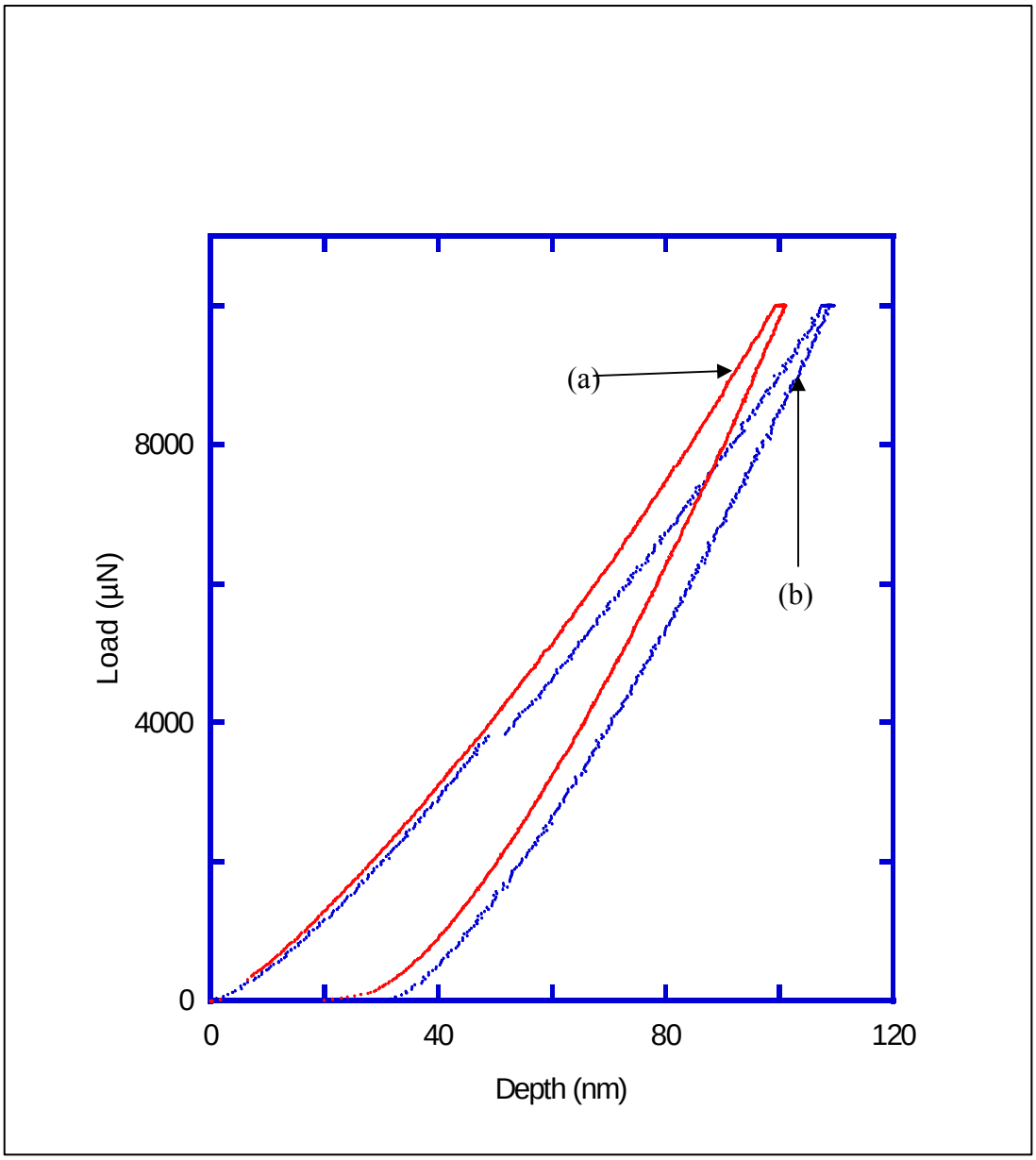

Figure 4.9. Load-Displacement Curve at 10 mN (a) Polycrystalline SiC (b) Single Crystal SiC

Figure 4.10 and Figure 4.11, shows the hardness and modulus values of respective SiC films at various loads obtained from nanoindentation tests. Reduced modulus values of the thin film obtained from the nanoindentation are calculated using the equation (11).

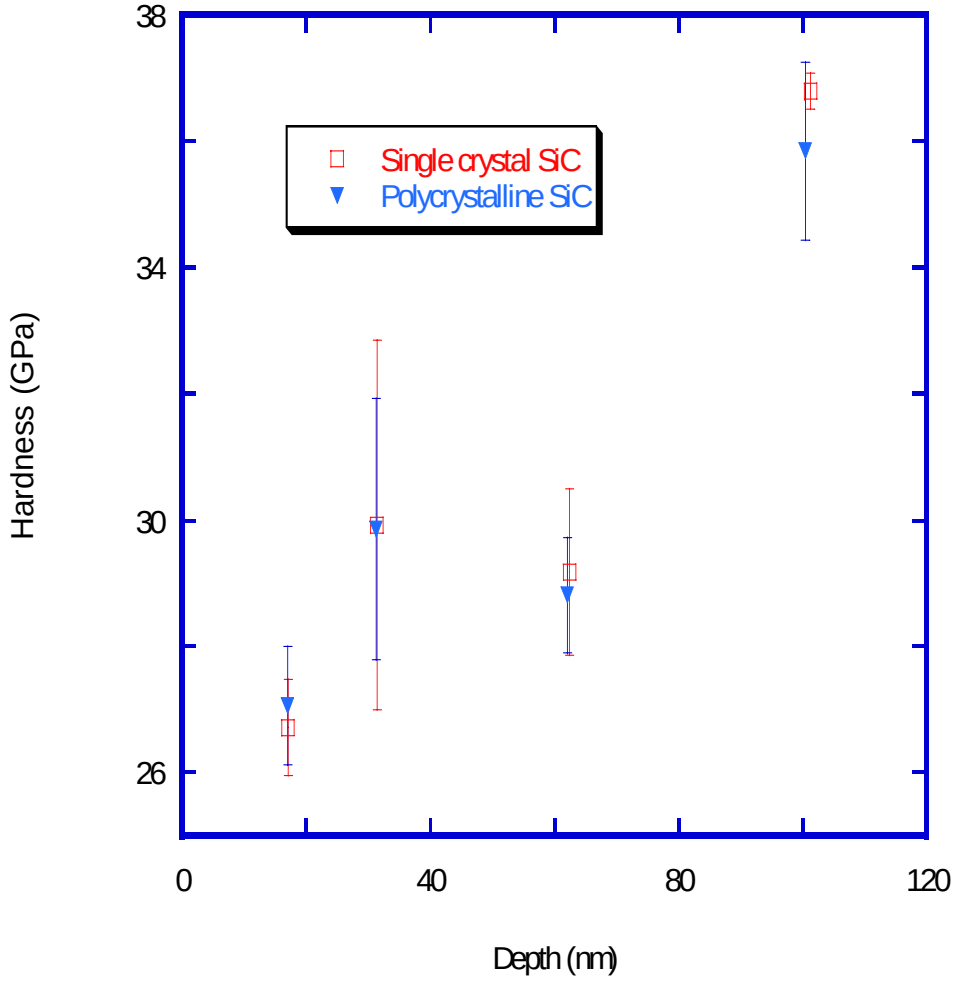

Figure 4.10. Hardness of Single Crystal and Polycrystalline SiC as a Function of Indentation Depth

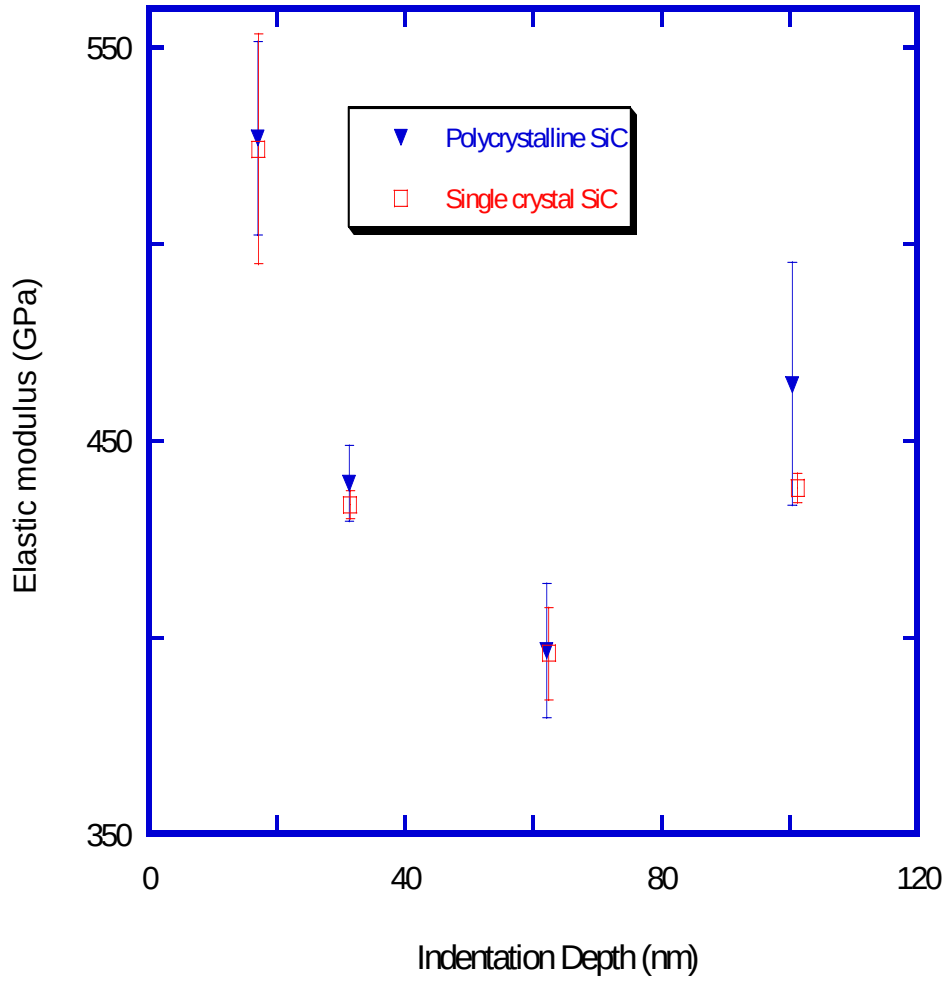

Figure 4.11. Modulus of Single Crystal and Polycrystalline SiC as a Function of Indentation Depth

Figure 4.12, Shows the load displacement curves for Lely-Platelet 15R- SiC (Bulk SiC), polycrystalline SiC, single crystal SiC and Si (100) at 10 mN. Table 2 gives the hardness and modulus values for 15R- SiC (Bulk SiC), polycrystalline SiC, single crystal SiC and Si (100) obtained using nanoindentation.

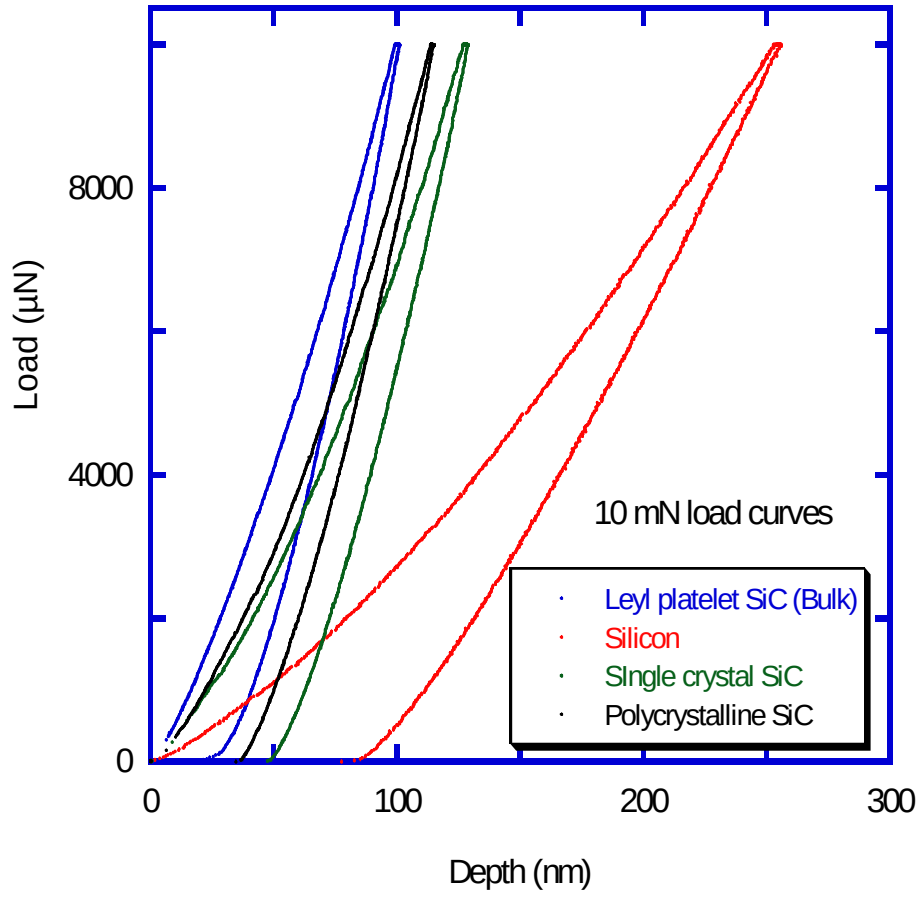

Figure 4.12. Load-Displacement Curves for Bulk SiC, Single Crystal, and Polycrystalline 3C-SiC Films and Bulk Si (100)

Table 2. Mechanical Properties of Single Crystal SiC, Single Crystal Si, Polycrystalline SiC and Bulk SiC (Lely Platelet SiC)

	Hardness (GPa)	Elastic Modulus (GPa)
Silicon (100)	12.46 $\pm$ 0.78	172.13 $\pm$ 7.76
Lely platelet 15R-SiC	42.76 $\pm$ 1.19	442 $\pm$ 16.34
Single crystal 3C-SiC	30 $\pm$ 2.8	410 $\pm$ 3.18
Polycrystalline 3C-SiC	32.69 $\pm$ 3.218	422 $\pm$ 16

4.2.3 Fracture Toughness Analysis

To determine the fracture toughness (K), low load transducer was replaced with high load transducer. The indentation procedure mentioned in Chapter 3 was followed at higher loads ranging from 100 mN to 500 mN.

Figures 4.13 and 4.14 show the microscopic images of cracks induced at higher loads in polycrystalline and single 3C-SiC films, respectively. Crack length was used to calculate the fracture toughness of the thin films using equation (13). The radial cracks were generated along the sharp corners of the Berkovich tip used for indentation. Table 3, shows the values of fracture toughness of respective SiC samples. The cause for the low values of fracture toughness in this case was due to the tip penetrating into the substrate.

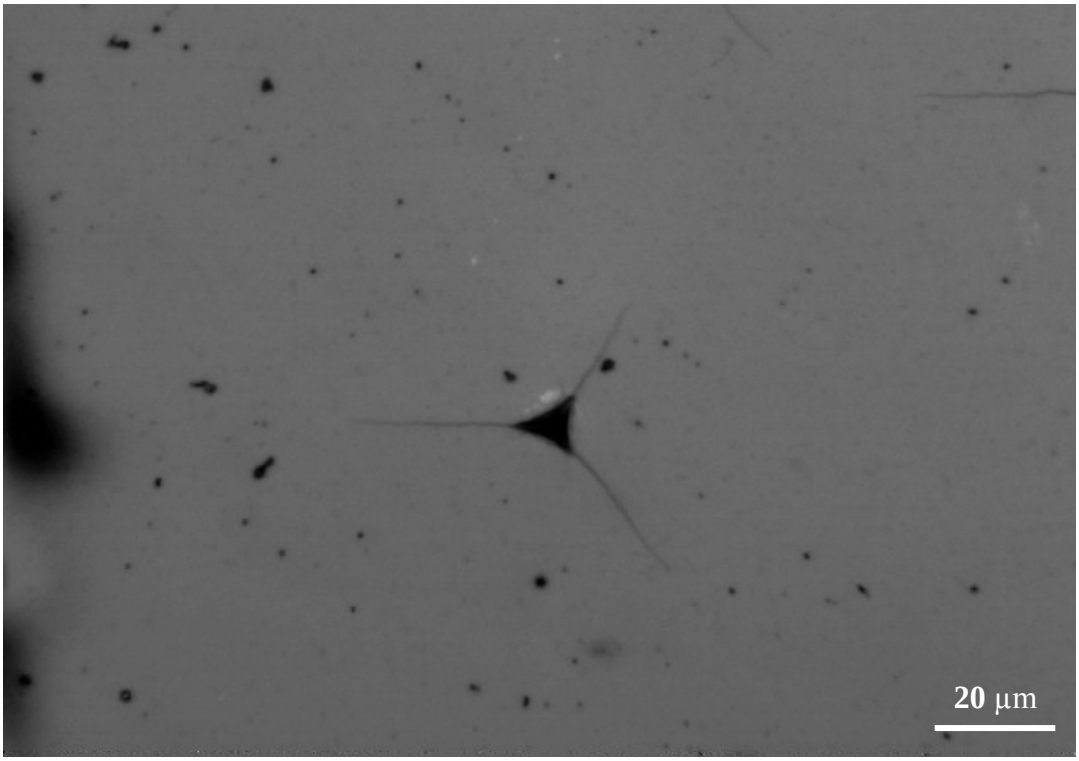

Figure 4.13. Radial Cracks in Polycrystalline SiC Film

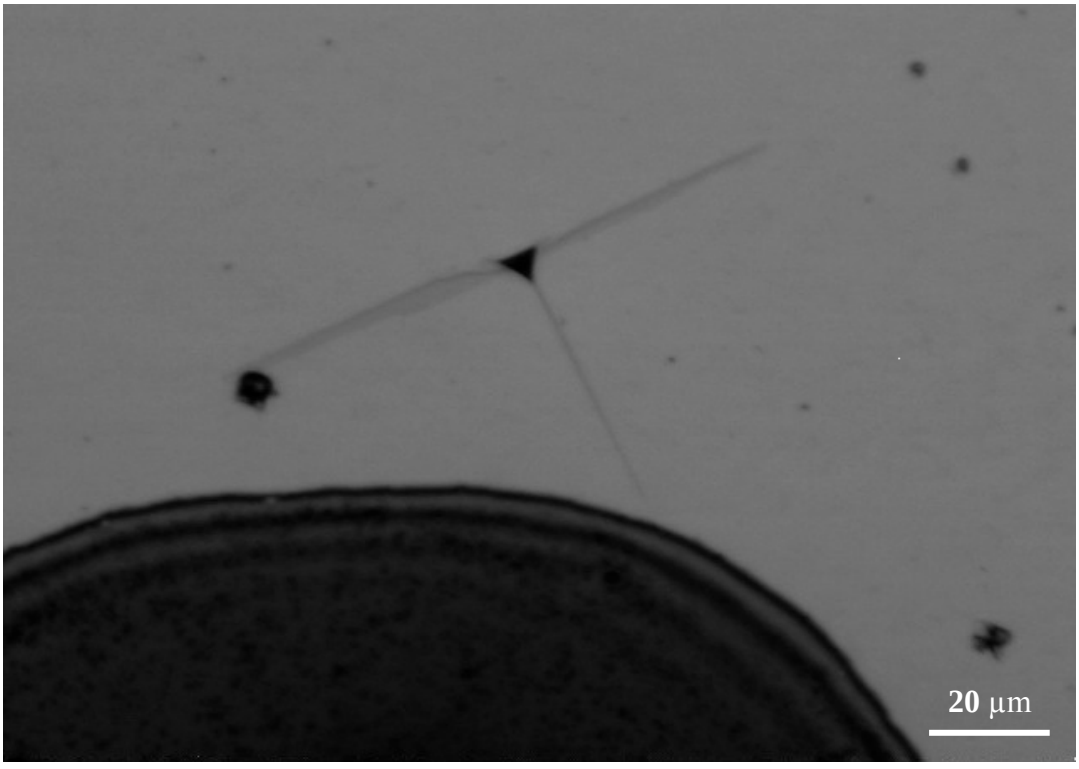

Figure 4.14. Radial Cracks in Single Crystal SiC Film

Table 3. Fracture Toughness Values for Single Crystal and Polycrystalline SiC

Material	Fracture Toughness (MPa√m)
Single Crystal SiC	1.58 ± 0.5
Polycrystalline SiC	1.48 ± 0.6
Bulk SiC	4.6
Bulk SiC (D.Yang and T.Anderson)	2.18

From Figure 4.13, we can see that the cracks of the single crystal SiC are propagating along the cubic planes. Same effect is not noticed in the polycrystalline SiC Figure 4.14, since they do not have specific cubic planes to further propagate the crack very easily.

CHAPTER 5

5.1 Conclusions and Recommendations

This chapter reviews the experimental results obtained and contains future recommendations for comparing mechanical properties nanoindentation data with other methods.

5.1.1 Conclusions

In this work, mechanical properties of the single crystal and polycrystalline 3C-SiC thin films were studied using Hysitron Triboindenter in the ambient environment. These films were deposited on silicon substrates by the chemical vapor deposition technique. Hardness and elastic modulus were measured using nanoindentation tests and compared with bulk SiC (Lely Platelet 15R-SiC) properties and the silicon substrate. The effect of surface roughness on polycrystalline 3C-SiC thin film mechanical properties was studied. The properties of rough polycrystalline SiC was compared with the smooth or polished sample. Fracture toughness of the films was determined from the indentation experiments.

5.1.2 Properties of SiC Films

Modulus and hardness values found from the nanoindentation tests for polycrystalline 3C-SiC films were 422 $\pm$ 16 GPa and 32.69 $\pm$ 3.218 GPa respectively, while single crystalline 3C-SiC films elastic modulus and hardness were 410 $\pm$ 3.18 GPa and 30 $\pm$ 2.8 GPa, respectively. Bulk SiC properties were found to be 442 $\pm$ 16.34 GPa for the elastic modulus and 42.76 $\pm$ 1.19 GPa for hardness. E and H for silicon substrate were found to be 172.13 $\pm$ 7.76 GPa and 12.46 $\pm$ 0.78 GPa, respectively. From the results one can observe that the mechanical properties of the Single and polycrystalline SiC films are relatively close to the bulk SiC.

5.1.3 Surface Roughness Effect

RMS roughness of as-deposited polycrystalline SiC was measured to be 53 nm approximately and topography images show that the peaks-to-valley depth was around 273 nm. This unevenness in the surface affected the measurement of the properties of the thin films. From the experiments, it was observed that H and E values were not comparable with bulk SiC, but did not affect the results. The SiC film surface was then polished to an RMS roughness of 2 nm approximately and the H and E values were compared with rough SiC film and bulk SiC. The H and E values of as-deposited SiC were measured, and found to be 260 $\pm$ 86.5 GPa and 18.92 $\pm$ 9.6 GPa respectively, after polishing the film.

5.1.4 Fracture Toughness of SiC Films

Fracture toughness of SiC films was studied using nanoindentation. Radial cracks were initiated by applying relatively higher loads using a sharp Berkovich diamond tip. Fracture toughness was calculated from the crack length and the values are found to be 1.58 ± 0.5 MPa√m for polycrystalline SiC and 1.48 ± 0.6 MPa√m for single crystal 3C-SiC films. These results were compared with fracture toughness for bulk SiC. From the fracture toughness values obtained for both the single and polycrystalline it can be noted that they have relatively low values compared to the bulk material. This low values can be attributed due to various reasons like, substrate effect or residual stress caused during the deposition of the SiC thin films on Si substrate.

5.2 Recommendations and Future Research

Additional experiment could be done to compare the hardness values obtained by nanoindentation with a scratch test results. To confirm the values of the fracture toughness, an in-depth analysis of the cubic planes need to be studied in order to explain the crack propagation in both single crystal and polycrystalline SiC. Nanoindentation tests could be conducted in wet environments to observe the changes in fracture toughness of these films.

REFERENCES

1. M Ohring, The Material science of Thin films, Academic press, 1991.

2. www.ifm.liu.se/matephys/new/SiC/

3. A. Klumpp, U. Schaber, H.L. Offereins, K. Ku¨ hl, H. Sandmair, Sensors and Actuators A 41–42, 310–316(1994).

4. N. Ledermann, J. Baborowski, P. Muralt, N. Xantopoulos, J.-M. Tellenbach, Surface and Coatings technology 125, 246-250 (2000).

5. www.lerc.nasa.gov/WWW/SiC/SiC.html

6. J. Musil, Surface and Coatings Technology 125, 322–330 (2000).

7. D. M. Cao, T. Wang, B. Feng, W. J. Meng, and K. W. Kelly, Thin Solid Films 398, 553, References 1(2001).

8. S. Prasad, T. Christenson, and M. Dugger, Adv. Mater. Process. 160, 30, 2002.

9. Y. Tian, A. F. Bastawros, C. C. H. Lo, A. P. Constant and A. M. Russell, B. A. Cook, Applied Physics Letters, volume 83, number 146 October 2003.

10. Xiao-An Fu, Jeremy L. Dunning, Christian A. Zorman, Mehran Mehregany, Sensors and Actuators A 119, 169–176 (2005).

11. K.L. Choy, Progress in Materials Science 48, 57–170 (2003).

12. S. Venkataraman, D. Kohlstedt, W.W. Gerberich, Metal-Ceramic Interfacial Fracture Resistance using the Continuous Microscratch Technique, Thin Solid Films, 223, pp. 69-275 (1993)

13. P. Benjamin, C. Weaver, Measurement of Adhesion of Thin Films, Proc. Soc. London, 254, pp. 163-176 (1960)

14. D. Beegan, S. Chowdhury, M.T. Laugier, Surface and Coatings Technology, 201, 5804 (2007).

15. R. Schwaiger and O. Kraft, Scripta Materialia, Vol. 41, No. 8, pp. 823–829, 1999

16. Jay S. Mitchell; Christian A. Zorman; Thomas Kicher; Shuvo Roy4; and Mehran Mehregany, Journal of Aerospace Engineering, 46-54, April (2003).

17. J.H. He, J.K. Luo, H.R. Le, D.F. Moore, Materials Science and Engineering A 423 134–142 (2006).

18. H.J. Lee, H.S. Choi , C.S. Han, N.K. Lee, G.A. Lee, T.H. Choi, Journal of Materials Processing Technology 187–188 ,241–244 (2007).

19. Kamili M. Jackson, Jeremy Dunning, Christian A. Zorman, Mehran Mehregany, William N. Sharpe, Jr., Journal of MicroElectroMechanical Systems, Vol. 14, No. 4, August 2005

20. B. Yuan, W.N. Sharpe Jr., Mechanical testing of polysilicon thin films with the ISDG, Exp. Tech. 21 32–35 (1997).

21. Kamili M. Jackson, Sensors and Actuators A 125 34–40(2005).

22. W.C. Oliver, G.M. Pharr, *An Improved Technique for Determining Hardness and Elastic Modulus using Load and Displacement Sensing Indentation Experiments*, J. Mat. Res. 7, pp. 1564-1580 (1992)

23. Antony C. Fischer Cripps, Nanoindentation, Springer-Verlag New York, LLC

24. W.A. Bonin and Hysitron Inc., Multi-dimension capacitive transducer, United states Patent, 5869751, 1999.

25. Hysitron Inc., 10025 Valley View Road, Minneapolis, MN, 55344, USA.

26. J.L.Hay, M.E. O'Hern, and W.C. Oliver, "The importance of contact radius for substrate-independent property measurement of thin films", Mat. Res. Soc. Symp. Proc. 522, pp 27-32 (1998).

27. E.S. Berkovich, "Three-faced diamond pyramid for micro-hardness testing", Ind. Diamond Rev. 11 127, pp.129-133 (1951).

28. www.nanoindentation.cornell.edu/Testing_Issues/Nanoindentation-testing_Issues.htm

29. A.A. Volinsky, W.W. Gerberich, *Nanoindentation techniques for assessing mechanical reliability at the Nanoscale*, Mico. Elect. Eng. 69, pp. 519-527 (2003)

30. N. Yu, A. Polycarpou, T. Conry, *Tip-radius Effect in Finite Element Modeling of Sub-50 nm Shallow nanoindentation*, Thin Solid Films 450 pp. 295-303 (2003).

31. Anstis GR, Chantikul P, Lawn BR, Marshall DB. J Am Ceram Soc; 64:533 (1981).

32. Daniel Casellas, Juame Caro, Sivia Molas, Jose M. Prado, Isaac Valls Acta Materialia 55, 4277-4286 (2007).

33. B.R.Lawn, A.G. Evans, and D.B.Marshall, "Elastic/ Plastic indentation damage in ceramics: the median/radial crack system," J. Am. Ceram. Soc. 63, pp. 574-581(1980).

34. H.Bei, E.P.George, J.L.Hay, and G.M. Pharr, "Influence of Indenter Tip Geometry on Elastic Deformation during Nanoindentation", The American Physical Society, July 2005.

35. S.Suresh, T.G. Nieh and B.W. Choi, Scr. Mater. 41, 951(1999).

36. W.W. Gerberich, J.C. Nelson, E.T. Lilleodden, P. Anderson and J.T. Wyrobek, Acta. Mater. 44, 3585 (1996).

37. K.L. Johnson, Contact Mechanics, Cambridge University press 1985.

38. Thesis S.Harvey, Electrical Engineering department, USF (2006).

39. W. Kern and D. A. Puotinen, *Cleaning solutions based on hydrogen peroxide for use in silicon semiconductor technology*, RCA Rev. Vol. 31, 187-206 (1970).